Available online at www.sciencedirect.com

SciVerse ScienceDirect

Geochimica et Cosmochimica Acta 113 (2013) 193–224

Geochimica et Cosmochimica Acta

www.elsevier.com/locate/gca

Multi-element isotopic analyses of presolar graphite grains from Orgueil

Manavi Jadhav [a,*], Ernst Zinner [b], Sachiko Amari [b], Teruyuki Maruoka [b,1], Kuljeet K. Marhas [b,2], Roberto Gallino [c,d]

[a] *Laboratory for Space Sciences and the Department of Earth and Planetary Sciences, Washington University, One Brookings Drive, St. Louis, MO 63130, USA*

[b] *Laboratory for Space Sciences and the Physics Department, Washington University, One Brookings Drive, St. Louis, MO 63130, USA*

[c] *Dipartimento di Fisica Generale, Universita di Torino, Via P. Giuria 1, I-10125 Torino, Italy*

[d] *INAF-Osservatorio Astronomico di Collurania, Via Maggini, 64100 Teramo, Italy*

Received 12 December 2011; accepted in revised form 15 January 2013; available online 4 February 2013

Abstract

We report C, N, O, Si, Al–Mg, K, Ca, and Ti isotopic analyses of presolar graphite grains from the Orgueil CI chondrite. NanoSIMS isotopic measurements were made on 345 grains from seven density fractions, with grain sizes >1 μm: low-density grains from OR1b, OR1c, and OR1d; and high-density grains from OR1f, OR1g, OR1h, and OR1i. In all fractions, except OR1b and OR1h, we found presolar graphite as demonstrated by the large range of $^{12}C/^{13}C$ ratios (4–2480) measured in individual grains. Some isotopic properties are dependent on density: low-density grains contain ^{18}O, ^{15}N, and ^{28}Si excesses, while the majority of high-density grains contain normal N and O, and are generally enriched in ^{29}Si and ^{30}Si. The ^{15}N, ^{18}O, and ^{28}Si excesses and very high derived isotopic ratios for the extinct radionuclides ^{26}Al, ^{41}Ca, and ^{44}Ti in low-density grains indicate an origin from supernovae. In order to explain the isotopic ratios measured in these grains, we present mixing scenarios between different layers of supernovae and discuss the limitations of various theoretical models. Silicon-30 and ^{12}C excesses in high-density grains and lower values for short-lived radionuclides (^{26}Al and ^{41}Ca) indicate an origin in asymptotic giant branch stars with low metallicities. Some supernova grains, with ^{44}Ca excesses, are also present amongst the high-density grains. Grains with low $^{12}C/^{13}C$ ratios (without evidence for ^{44}Ti) and large excesses in $^{42,43}Ca$ and $^{46,47,49,50}Ti$ probably originate from post-asymptotic giant branch stars, that have suffered a very late thermal pulse, and can achieve low $^{12}C/^{13}C$ ratios and large neutron capture signatures in Ca and Ti isotopes.

We conclude that most low-density graphite grains originate from supernovae while high-density graphite grains have multiple stellar sources: low-metallicity and born-again asymptotic giant branch stars, Type II supernovae, and possibly, J-type stars.

* Corresponding author. Present address: Hawai'i Institute of Geophysics and Planetology, University of Hawai'i at Mānoa, 1680 East-West Road, POST 602, Honolulu, HI 96822, USA.

E-mail address: manavi@higp.hawaii.edu (M. Jadhav).

[1] Present address: Graduate School of Life and Environmental Sciences, University of Tsukuba, 1-1-1 Tennodai, Tsukuba City, Ibaraki 305-8572, Japan.

[2] Present address: Physical Research Laboratory, Navrangpura, Ahmedabad 380009, Gujarat, India.

0016-7037/$ - see front matter © 2013 Elsevier Ltd. All rights reserved.
http://dx.doi.org/10.1016/j.gca.2013.01.018

1. INTRODUCTION

Amari et al. (1990) isolated the first presolar graphite grains from the Murchison CM2 meteorite by identifying the grains to be carriers of the exotic noble gas component Ne-E(L) (almost pure ^{22}Ne). Subsequently, extensive isotopic studies were carried out on the Murchison density fractions: KE1 and KE3 (1.6–2.05 g cm^{-3}), KFA1 (2.05–2.10 g cm^{-3}), KFB1 (2.10–2.15 g cm^{-3}), and KFC1 (2.15–2.20 g cm^{-3}) (Amari et al., 1990, 1995a, 2012; Hoppe et al., 1995; Zinner et al., 1995; Travaglio et al., 1999). All isotopically identified presolar graphite grains in Murchison seem to be spherical, with diameters >1 μm (ranging up to ~20 μm). Structural and isotopic properties of Murchison presolar graphite vary with density (Amari et al., 1995b; Hoppe et al., 1995). More recently, graphite grains were isolated from the Orgueil CI chondrite (Jadhav et al., 2006). Similar spherical grains were identified and studied in different density fractions of Orgueil (Jadhav et al., 2006, 2008). In general, graphite grains from Orgueil appear to be rather similar to those from Murchison, both morphologically and in their isotopic properties.

Many low-density graphite grains from both meteorites exhibit evidence for an origin in Type II supernovae. Their isotopic properties are similar to those of SiC X grains, which are known to originate from core-collapse supernovae (Amari et al., 1992). They have large excesses in ^{15}N, ^{18}O, and ^{28}Si (Amari et al., 1995b; Travaglio et al., 1999; Jadhav et al., 2006). Many of the low-density grains have high initial inferred ^{26}Al/^{27}Al ratios (^{26}Al $\tau_{1/2} = 7.35 \times 10^5$ a) and some show evidence for the initial presence of the short-lived radioisotope ^{44}Ti ($\tau_{1/2} = 60$ a) in the form of large ^{44}Ca excesses (Nittler et al., 1996), and of ^{41}Ca ($\tau_{1/2} = 1.03 \times 10^5$ a) in the form of large excesses in ^{41}K (Amari et al., 1996). Travaglio et al. (1999) were able to reproduce these major isotopic signatures of low-density grains by performing mixing calculations of theoretical predictions for the compositions of the different layers of Type II SNe. Furthermore, Croat et al. (2003) found iron-metal phases and TiC subgrains in low-density graphites that also exhibit SN signatures. On the other hand, low-metallicity, asymptotic giant branch (AGB) stars seem to be the source of a large fraction of high-density graphite grains. One of the *s*-process components of Kr, Kr-SH, with a high ^{86}Kr/^{82}Kr ratio, resides in the high-density fraction of Murchison graphites and is believed to originate from AGB stars (Amari et al., 1995a). Additional evidence for AGB graphites came from TEM studies by Croat et al. (2005). These authors found that high-density grains from Murchison contain subgrains rich in the *s*-process elements Zr, Mo, and Ru, indicating an AGB origin. High-density graphites were also found to have large ^{30}Si excesses that are correlated with high ^{12}C/^{13}C ratios (Amari et al., 2005; Jadhav et al., 2006). Some low-metallicity AGB stars that do not undergo cool bottom processing, a mixing scenario that was invoked to explain low ^{18}O/^{16}O ratios in oxide grains (Wasserburg et al., 1995a), and low ^{12}C/^{13}C ratios and large ^{30}Si excesses in SiC Z grains (Hoppe et al., 1997; Nollett et al., 2003) can produce high ^{12}C/^{13}C ratios. Carbon-12 and ^{29,30}Si from the He intershell are mixed into the envelope by third dredge-up (TDU) during the thermally pulsing phase (Busso et al., 1999; Zinner et al., 2006a), ultimately making the star C-rich. Such a C > O environment is ideal for the condensation of graphite grains (Lodders and Fegley, 1997). Also, recent coordinated SIMS and noble gas studies (He and Ne isotopes) by Heck et al. (2009) and Meier et al. (2012) on high-density graphites from Murchison also confirm supernovae and low-metallicity AGB stars as the stellar sources for some of these grains. There is also some marginal evidence for grains from born-again AGB stars, J-type carbon stars, and novae.

The stellar source(s) of graphite grains with very low ^{12}C/^{13}C ratios still remains a matter of debate. The low- and high-density graphite grains from Murchison and Orgueil both contain a minor population of grains that have ^{12}C/^{13}C ratios of ~10 and lower. A recent study of high-density (OR1f – 2.02–2.04 g cm^{-3}) graphite grains from Orgueil (Jadhav et al., 2008) found extremely anomalous Ca and Ti ratios in some grains with ^{12}C/^{13}C ratios <20. These anomalies can only be explained by pure nucleosynthetic He-shell components of AGB stars. Born-again AGB stars, like Sakurai's object (V4334 Sgr), have low ^{12}C/^{13}C (~4) and exhibit enhanced *s*-process elemental abundances (Asplund et al., 1997, 1999). Jadhav et al. (2008) concluded that born-again AGB stars are likely sources of such graphite grains.

Here we give a comprehensive report on 345 Orgueil graphites and a discussion of their nucleosynthetic sources. All the data presented in this paper are available in an electronic appendix (Appendix Table A6). This paper is an extension of previous publications, Jadhav et al. (2006, 2008), and conference abstracts. It also provides detailed experimental procedures that were not reported in previous publications. We discuss the stellar sources of the graphite grains studied here by comparing the isotopic data with theoretical nucleosynthesis calculations and also outline the various limitations of these models.

2. EXPERIMENTAL METHODS

2.1. Chemical and physical separation of the graphite grains

The separation procedure used for this study was based on the procedure developed for Murchison graphite by Amari et al. (1994).

The Orgueil sample was obtained from the National Museum of Natural History in Paris. 24.16 g of the meteorite was treated with a mixture of toluene and methanol (4 times) to remove 0.57 g (~2.35% of original sample) of soluble organic matter. Silicates were then dissolved using alternating treatments with 10 M HF–1 M HCl and 6 M HCl (14 cycles). Each dissolution cycle was carried out at 70 °C for 15 h. The resulting residue was washed with 6 M HCl–0.6 M H_3BO_3 to remove insoluble fluorides. Washing was repeated twice at room temperature and thrice at 70 °C. The residue was subsequently treated with a mixture of 2 N H_2SO_4–0.5 N $Na_2Cr_2O_7$ at 75 °C for 20 h to oxidize the remaining reactive macromolecular organic matter. Unfortunately, we later learned that this treatment did not remove all the insoluble organic matter (IOM), as it did

during the Murchison separation. It has not yet been determined why the chemical separation failed to remove this material in Orgueil. Nanodiamonds were then extracted from the sample using the standard colloidal separation technique developed by Lewis et al. (1989). This treatment left behind a sediment of graphite, SiC, some oxides, and left-over IOM, and was further separated according to density by using sodium polytungstate, $Na_6(H_2W_{12}O_{40})$ (SPT) (Amari et al., 1994). The separation resulted in ten final density fractions of carbonaceous material. The lightest density fraction, OR1a (<1.59 g cm^{-3}), contains organic matter and the heaviest fraction, OR1j (>2.3 g cm^{-3}), contains SiC and oxide grains. At least a few of the remaining eight density fractions were expected to contain presolar graphite. These eight fractions were then further centrifuged and separated according to size with a lower cutoff of 1 μm. Since all the presolar graphite grains that carry Ne-E(L) in Murchison have diameters >1 μm, only those fractions were studied.

2.2. Grain-mount nomenclature

The eight different density fractions of the Orgueil graphites studied here are listed in Table 1. We introduce a new nomenclature to name the grains. Each grain label contains the name of the meteorite, the grain-size fraction, the density fraction, the analysis mount number, and finally, the grain number on that particular mount. For example, the grain label OR1d2m-4 indicates the following: OR = Orgueil, 1d = grains larger than 1 μm from the "d" density fraction (1.75–1.92 g cm^{-3}), 2m = second mount of grains from this density fraction that were analyzed for their isotopic compositions and 4 = the grain number on this mount.

2.3. Sample preparation

The initial set of grain mounts (OR1(b,c,d,e,f,g,h,i)1m) were prepared by suspending material from each density fraction in a solution of water and isopropanol (1:4). These suspensions were then mixed well in an ultrasonic bath, and small amounts (0.15–0.4 μl at a time) were deposited on high-purity gold foil mounts that are custom-made for the NanoSIMS.

Unfortunately, the large amount of insoluble macromolecular carbon that remained unoxidized during the separation caused a problem during measurements. Graphite grains are often found embedded in this material that covers areas of up to about 500 μm^2 on a grain mount. During the NanoSIMS measurements, the Cs^+ primary beam can be focused onto the central portion of the grain, thus reducing secondary ion contribution from the surrounding macromolecular carbon. However, the problem becomes inhibiting when the larger O^- primary beam is used to measure positive secondary ions and no secondary electron images are available to navigate the mount. In this case, the total ion count is used to locate grains. Grains embedded in macromolecular carbon become impossible to distinguish from their surroundings and ionic contributions from the surrounding material cannot be avoided.

Subsequent mounts (OR1d2m, 3m, 4m; OR1f2m) were prepared by picking grains with a micromanipulator and transferring them to separate NanoSIMS gold-foil mounts. Isolating the grains reduces contamination from the surrounding material and also makes it easier to locate them for future analyses. We picked larger grains (>2 μm) for analyses because these graphites are intended to be part of an extensive correlated study to measure the isotopes of light, selected elements up to Ni with the NanoSIMS, and of heavy (>Ni) elements with resonance ionization mass spectrometry (RIMS). Larger grains are more likely to survive extensive sputtering. The grain mounts were coated with a thin (~10–20 nm) layer of gold to prevent the grains from falling off the mount.

Various materials were deposited on each mount to aid in tuning of the secondary ion beam in the NanoSIMS and serve as isotopic calibration standards. Terrestrial graphite deposited from a colloidal suspension (DAG) was used as the C isotope standard for all the mounts, except OR1d4m, for which synthetic SiC was used. Fine-grained matrix material from Murchison was used as a standard for O isotopes. Synthetic SiC and SiC–Si_3N_4 grains were used as standards for Si and N isotopic measurements, respectively. We used Burma spinel ($MgAl_2O_4$) for Al–Mg isotopes and perovskite ($CaTiO_3$) grains as standards for Ca, K, and Ti isotopes.

2.4. EDX analyses and grain mount documentation

Carbonaceous grains were located and identified by energy dispersive X-ray (EDX) analysis with a JEOL-840A

Table 1
Different density fractions of Orgueil, the grain mounts that were analyzed, and the distribution of $^{12}C/^{13}C$ ratios in the density fractions.

Density fraction	Density type	Density (g cm^{-3})	Mounts analyzed	Number of grains analyzed	Group 1: $^{12}C/^{13}C < 20$	Group 2: $20 < {}^{12}C/^{13}C < 80$	Group 3 (normal): $80 < {}^{12}C/^{13}C < 100$	Group 4: $^{12}C/^{13}C > 100$
OR1b	LD	1.59–1.67	OR1b1m	22	–	–	100%	–
OR1c	LD	1.67–1.75	OR1c1m	7	–	1 grain	5 grains	1 grain
OR1d	LD	1.75–1.92	OR1d1m,2m,3m,4m	128	16%	16%	45%	23%
OR1f	HD	2.02–2.04	OR1f1m,2m	109	13%	4%	10%	73%
OR1g	HD	2.04–2.12	OR1g1m	52	13%	12%	29%	46%
OR1h	HD	2.12–2.16	OR1h1m	18	–	–	100%	–
OR1i	HD	2.16–2.30	OR1i1m	9	1 grain	1 grain	3 grains	4 grains

Note: LD = low-density graphite grains; HD = high-density graphite grains.

SEM. Candidate grains were selected on the basis of high C content and morphological features characteristic of Murchison graphite, either spherical with a platy 'onion' or knobby 'cauliflower' appearance (Hoppe et al., 1995). Mean grain sizes were also determined in the SEM. For irregularly shaped grains we used the formula for ellipsoids to determine the effective diameter, $D = (A * B^2)^{1/3}$, where A and B are the major and minor axes, respectively. Secondary electron images were obtained with the JEOL-840A SEM and field emission SE images with the PHI 700 Auger Nanoprobe at Washington University (Fig. 1).

2.5. NanoSIMS analysis

The initial characterization of the grains in the SEM was followed by SIMS isotopic analysis with the Washington University Cameca NanoSIMS 50. Typical primary beam sizes and currents used for these measurements were ~100 nm and ⩽1 pA, respectively, for the Cs^+ beam and ~300 nm and ~20 pA, respectively, for the O^- beam. The primary beams were always used in raster mode. The raster size depended on grain size and was adjusted such that the beam avoided the periphery of the grain in order to reduce macromolecular contamination from the mount and edges. Isotopic measurements were carried out in five stages on each mount. Appendix Table A1 gives a list of the measurement stages, the secondary ions being detected in multicollection mode (Phases 1–3) and combined mode (multicollection combined with magnetic peak-jumping; Phases 4 and 5), and the mounts on which these measurements were carried out.

2.5.1. C, N, O, Si isotopes

The first stage involved measuring C isotopes in combination with either N, O or Si isotopes simultaneously (Appendix Table A1). The remaining two elements were

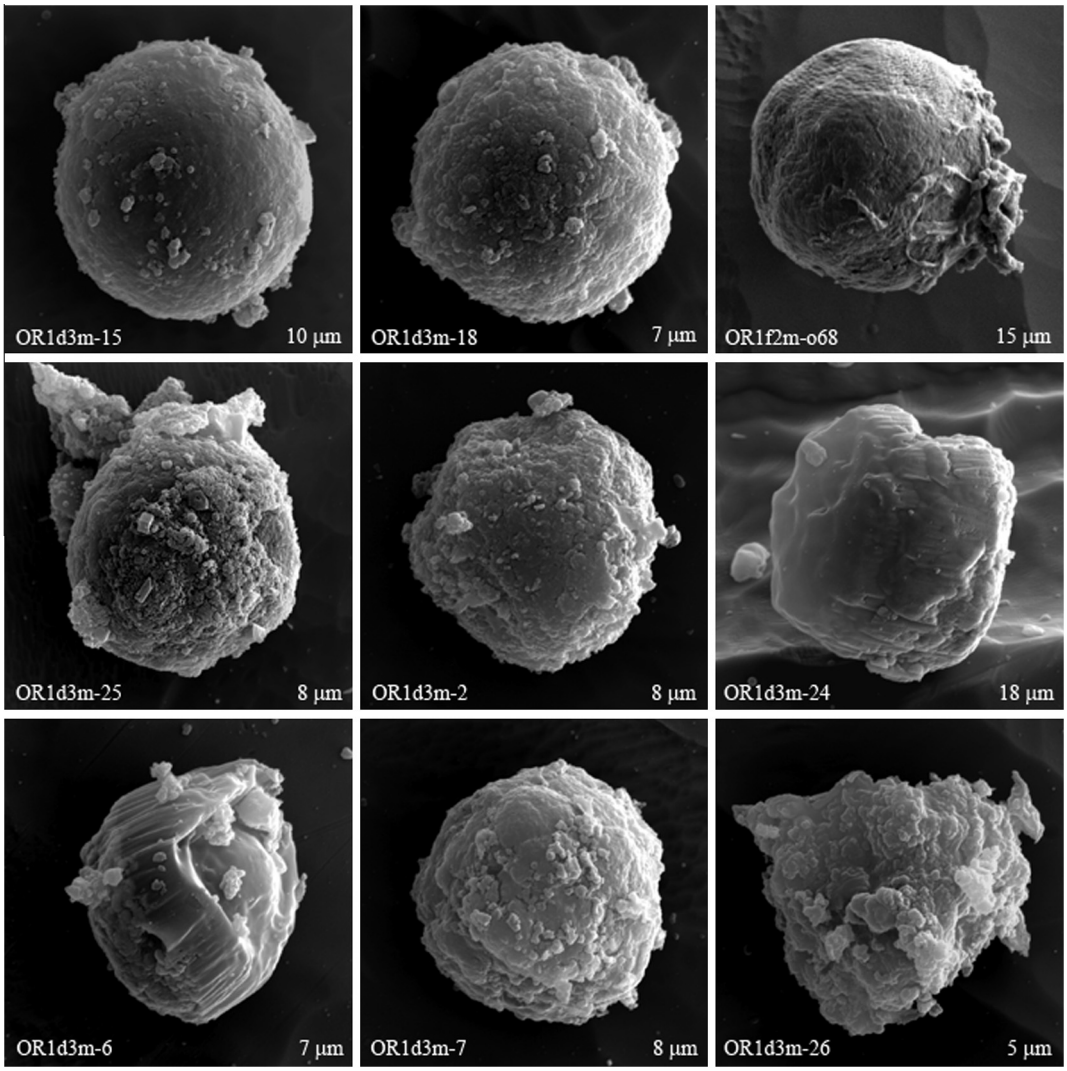

Fig. 1. Secondary electron images of graphite grains from Orgueil taken with the PHI 700 Auger Nanoprobe. There is a distinct lack of cauliflower grains (see Hoppe et al., 1995) among the Orgueil density separates. Grain names and diameters (in µm) are indicated for the individual grains.

measured in stage two. Analyses in the first two stages used a Cs^+ primary beam to produce the secondary ions $^{12}C^-$, $^{13}C^-$, $^{12}C^{14}N^-$, $^{12}C^{15}N^-$, $^{16}O^-$, $^{18}O^-$, $^{28}Si^-$, $^{29}Si^-$, and $^{30}Si^-$. All measurements, including those of positive secondary ions, were carried out at sufficiently high mass resolution to resolve all significant molecular interferences, e.g., $^{12}C^{14}N^-$ from $^{13}C_2^-$ and $^{12}C^{13}CH^-$ at mass 26, and $^{12}C^{15}N^-$ from $^{13}C^{14}N^-$ at mass 27. Grain measurements were bracketed by standard measurements at regular intervals (every 5–10 grains). In addition, mass peaks were centered before every grain and standard measurement. Possible changes in the primary ion beam current do not affect isotopic ratios since all the isotopes are measured simultaneously.

The isotopic data were reduced by normalizing the measured ratios to the average ratios of the standard grains. The standard ratios used in this study are: measured values of $^{12}C/^{13}C = 91.2$ for DAG and 92.6 for SiC, and terrestrial values of $^{14}N/^{15}N = 272$ and $^{16}O/^{18}O = 499$. Silicon isotopic ratios were expressed as δ-values, deviation from the normal ratios in permil (‰). Delta notation is defined as: $\delta^aX\ (‰) = [(^aX/^bX)_{meas}/(^aX/^bX)_{std} - 1] \times 1000$. Measurement errors were usually dominated by counting statistics and Poisson errors of the isotopic ratios of unknown grains were appropriately combined with the standard deviation of repeated measurements on the standards to obtain 1σ errors for each measurement.

2.5.2. Al–Mg isotopes

In phase 3 of the analyses, the positive secondary ions $^{12}C^+$, $^{24}Mg^+$, $^{25}Mg^+$, $^{26}Mg^+$, and $^{27}Al^+$, produced with an O^- primary beam, were detected simultaneously. Positive ions of ^{12}C were monitored in order to locate the grains. Burma spinel grains were measured as standards to obtain the Mg isotopic ratios and the $^{27}Al/^{24}Mg$ ratios in the graphite grains. We assumed atomic Al/Mg = 2 for the spinel grains. In grains with normal (within uncertainties) $^{25}Mg/^{24}Mg$ ratios, large ^{26}Mg excesses are assumed to be from the decay of ^{26}Al. Addition of isotopically normal Mg can reduce the ^{26}Mg excess relative to ^{24}Mg but it also reduces the $^{27}Al/^{24}Mg$ ratio by the same factor. Thus, contamination by terrestrial Mg does not affect the inferred $^{26}Al/^{27}Al$ ratio. In contrast, ^{27}Al contamination can decrease the calculated $^{26}Al/^{27}Al$ ratio, and hence, special care was taken to sputter away terrestrial Al contamination and to avoid Al hotspots on the sample mount. All inferred $^{26}Al/^{27}Al$ ratios should be considered to be lower limits because of the possibility of Al contamination. The ^{26}Mg excesses ($^{26}Mg_{excess}$) were calculated directly from the ion counts: $^{26}Mg^+_{excess} = {}^{26}Mg^+ - (^{26}Mg^+/^{24}Mg^+)_{std} \times {}^{24}Mg^+$, where $(^{26}Mg^+/^{24}Mg^+)_{std}$ is the ratio measured on the standard spinel grains. The inferred $^{26}Al/^{27}Al$ ratios were then calculated by: $^{26}Al/^{27}Al = \Gamma \times {}^{26}Mg^+_{excess}/^{27}Al^+$, where Γ is the sensitivity factor for Al and Mg secondary ion yields determined from the spinel grains. The value of Γ varied between 1.8 and 2.3 for different measurement sessions.

2.5.3. K and Ca isotopes

The K, Ca, and Ti measurements were carried out with an O^- primary beam in a combination of peak-jumping and multi-collection modes (see Appendix Table A1). Positive secondary ions of ^{39}K, ^{41}K, and ^{43}Ca (B field 1) and ^{12}C, ^{40}Ca, ^{42}Ca, ^{44}Ca, and ^{48}Ti (B field 2) were measured to obtain K and Ca ratios. Since the intrinsic concentration of K in graphite grains is expected to be very low because of its high volatility, and all the terrestrial K is probably from contamination, we attribute ^{41}K excesses seen in some graphite grains to be due to the decay of ^{41}Ca ($\tau_{1/2} = 1.03 \times 10^5$ a) (Amari et al., 1996). We calculated the initial $^{41}Ca/^{40}Ca$ ratios in the grains, as we did the inferred $^{26}Al/^{27}Al$ ratios: $^{41}Ca/^{40}Ca = \Gamma \times {}^{41}K^+_{excess}/^{40}Ca^+$, where the sensitivity factor, $\Gamma = 0.462$, was measured on NIST 610. The Ca isotopic ratios are expressed as δ-values. In grains with ^{44}Ca excesses that are larger than the $^{42,43}Ca$ excesses, we attribute the excesses to be from the decay of the short-lived radionuclide ^{44}Ti, because all existing models for AGB and SN nucleosynthesis predict $^{42,43}Ca$ excesses to be larger than ^{44}Ca excesses from neutron capture. The inferred $^{44}Ti/^{48}Ti$ ratios were calculated similar to the $^{26}Al/^{27}Al$ and $^{41}Ca/^{40}Ca$ ratios: $^{44}Ti/^{48}Ti = \Gamma \times {}^{44}Ca^+_{excess}/^{48}Ti^+$, where we used $\Gamma = 0.353$ (Lin et al., 2010). The $^{48}Ti^+$ signal was corrected for a contribution from $^{48}Ca^+$ under assumption of a normal $^{40}Ca/^{44}Ca$ ratio (47.153 from Niederer and Papanastassiou, 1984).

2.5.4. Ti isotopes

Three magnetic field settings were used to measure Ti isotopes: B_1: $^{46}Ti^+$, $^{48}Ti^+$, and $^{50}Ti^+$; B_2: $^{47}Ti^+$, $^{49}Ti^+$, and $^{51}V^+$; and B_3: $^{12}C^+$, $^{40}Ca^+$, $^{48}Ti^+$, $^{50}Ti^+$, and $^{52}Cr^+$. Vanadium-51 and ^{52}Cr were used to correct the ^{50}Ti signal for isobaric interferences from ^{50}V and ^{50}Cr, and ^{40}Ca was measured to correct for Ca interferences at masses 46 and 48. These interferences cannot be resolved in the NanoSIMS. Abundances of ^{46}Ca and ^{48}Ca are sufficiently low that we do not expect these interferences to produce significant anomalies. Corrections were applied by assuming normal or terrestrial $^{46}Ca/^{40}Ca$ and $^{48}Ca/^{40}Ca$ ratios. A larger than normal $^{48}Ca/^{40}Ca$ ratio will result in a deficit in the Ti isotopic ratios relative to ^{48}Ti. In such cases, the observed excesses in these Ti isotopic ratios will be lower limits. We also assume that the ^{50}Cr interference to the ^{50}Ti signal is entirely from terrestrial Cr because the grains inherit large quantities of terrestrial Cr from the oxidizer, $Na_2Cr_2O_7$, which is used during the chemical separation procedure for graphite grains. The following terrestrial values were used for the corrections: $^{40}Ca/^{44}Ca = 47.153$, $^{48}Ca/^{44}Ca = 0.088727$, $^{46}Ca/^{44}Ca = 0.00152$ (Niederer and Papanastassiou, 1984), $^{50}Cr/^{52}Cr = 0.051859$ (Shields, 1966) and $^{50}V/^{51}V = 0.002503$ (Flesch et al., 1966).

3. RESULTS

We defined low-density (LD) graphites to be from fractions OR1b, OR1c, and OR1d (1.59–1.92 g cm^{-3}), while grains from OR1f, OR1g, OR1h, and OR1i (2.02–2.30 g cm^{-3}) fractions are the high-density (HD) graphites (Table 1).

Most of the graphite grains from the Orgueil density fractions resemble HD Murchison presolar graphites (Hoppe et al., 1995; Fig. 1). They are spherules with smooth

surfaces and a platy, onion-like morphology. Very few grains with the cauliflower-type morphology were found. Cauliflower grains are the dominant morphology in the LD fractions of Murchison (Hoppe et al., 1995). Some potato-shaped presolar graphite grains with smooth surfaces were found in the Orgueil fractions. The range of grain diameters in the LD fraction is 1–18 μm and 1–35 μm in the HD fraction. The average LD grain size is 5 μm (median = 4) and between 5–6 μm (median = 5) for HD grains. However, amongst the LD grains about 50% of the grains are 1–4 μm in size, while 45% have sizes within this range amongst the HD grains. Thus, there are a slightly larger number of HD grains with sizes >4 μm than LD grains.

3.1. Isotopic compositions of the grains

3.1.1. Distribution of $^{12}C/^{13}C$ ratios

Grains from five (OR1c, d, f, g, i) of the seven density fractions analyzed were found to have isotopically anomalous carbon. There is no well-established solar $^{12}C/^{13}C$ ratio hence we assume the ratio of ~89 (Lodders, 2003). Fig. 2 displays histograms of the $^{12}C/^{13}C$ ratios in each density fraction and those of C stars in the galaxy (Lambert et al., 1986). The $^{12}C/^{13}C$ ratios of the grains in these fractions vary over a large range, from ~4 to 2500. We use the four "groups" described by Hoppe et al. (1995) to divide the grains: (1) Grains that are highly enriched in ^{13}C, with $^{12}C/^{13}C$ ratios smaller than 20, (2) Grains moderately ^{13}C-enriched, whose $^{12}C/^{13}C$ ratios are between 20 and 80, (3) Normal or close-to-solar $^{12}C/^{13}C$ ratios between 80 and 100, and (4) Grains containing isotopically light carbon with $^{12}C/^{13}C$ ratios greater than 100. Table 1 lists the C isotope distribution of the different populations of these grains within each density fraction based on the classification scheme described above.

Thus, we found that: (1) all the grains analyzed from the OR1b and OR1h density fractions are normal in C isotopic compositions and do not show the large variations that are

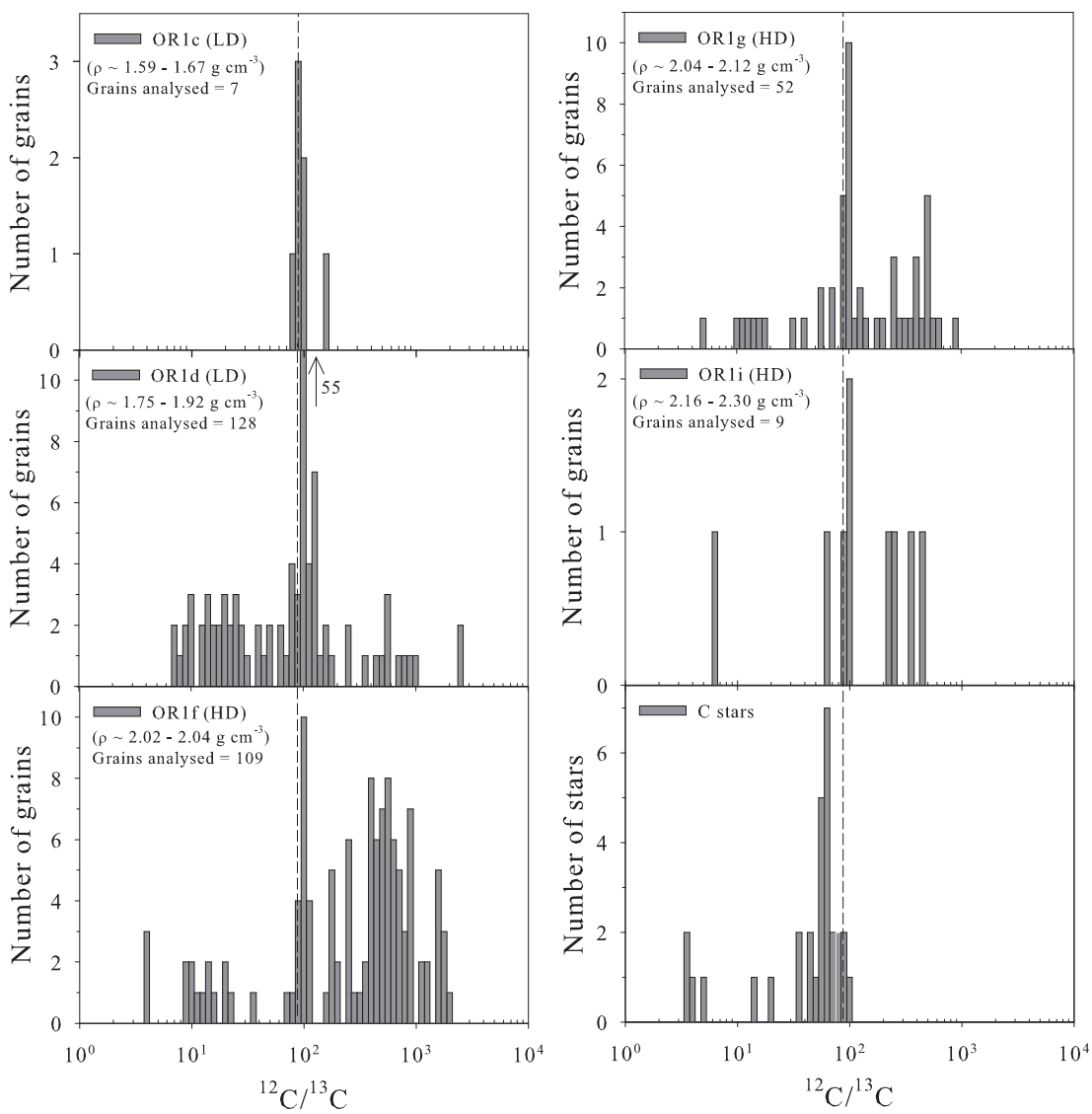

Fig. 2. The distribution of $^{12}C/^{13}C$ ratios of graphite grains from different density fractions of Orgueil. These ratios are compared to the C ratios measured in the atmospheres of carbon stars (Lambert et al., 1986). The solar $^{12}C/^{13}C$ ratio of ~89 is indicated by the dashed lines.

expected in presolar graphite (Hoppe et al., 1995); (2) grains with isotopically light C are more abundant in the HD fractions while grains with heavy C are more abundant in the LD fractions, and (3) a minor population (~15%) of grains with $^{12}C/^{13}C < 20$ is observed in all the fractions denser than OR1c. A similar density dependence of C isotopic ratios is seen in the Murchison graphites (Hoppe et al., 1995).

3.1.2. Nitrogen isotopes

In this study, we assume the $^{14}N/^{15}N$ ratio of 272 (Junk and Svec, 1958) to be the normal ratio. We use this ratio and not the true solar value (~459), recently measured by Marty et al. (2011) in Genesis solar wind samples, in order to facilitate comparison with old Murchison graphite data. Renormalizing the data with the newly measured solar value will not affect the discussion and conclusions of this paper.

Compared to carbon isotope ratios, the $^{14}N/^{15}N$ ratios in the LD density fractions exhibit a relatively limited range (Fig. 3a); they are normal in most of the HD grains (Fig. 3b). Both, OR1c and 1d contain grains with ^{15}N excesses relative to terrestrial $^{14}N/^{15}N$ (Fig. 3a). One OR1c grain (OR1c1m-6) has $^{14}N/^{15}N$ ~135, and while numerous OR1d grains are slightly ^{15}N-enriched ($^{14}N/^{15}N$ ratios between 272 and 200), only 17 grains have $^{14}N/^{15}N$ ratios between 200 and 100 and 5 have $^{14}N/^{15}N$ ratios less than 100. The largest ^{15}N excess was observed in grain OR1f1m-o67 ($^{14}N/^{15}N$ ~50).

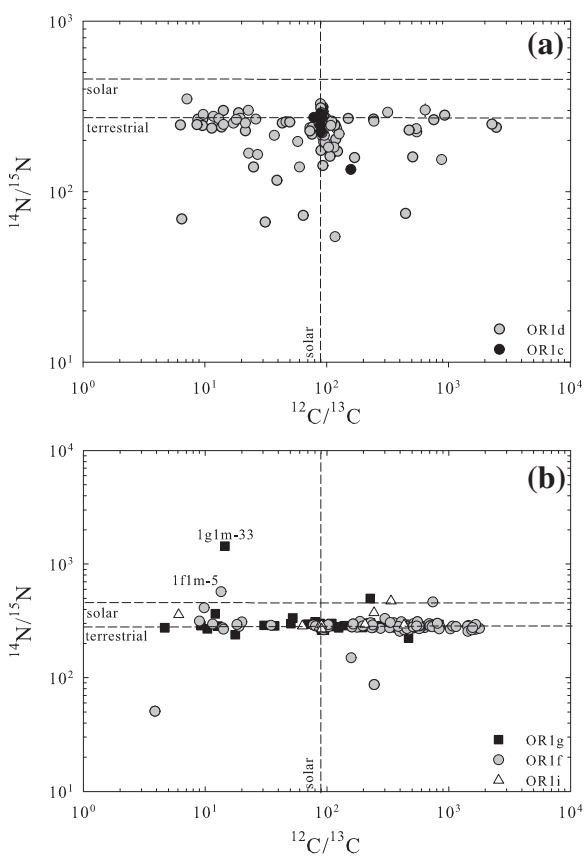

Fig. 3. (a) Carbon and nitrogen isotopic ratios of LD graphites from the OR1c and OR1d fractions. (b) $^{12}C/^{13}C$ and $^{14}N/^{15}N$ ratios of HD graphites from the OR1f, OR1g, and OR1i fractions. Dashed lines denote normal isotopic ratios (solar $^{12}C/^{13}C$ ~89; terrestrial $^{14}N/^{15}N$ ~272 and solar $^{14}N/^{15}N$ ~459). Error bars are 1σ.

The vast majority of grains from the HD fractions, OR1f, 1g, and 1i have terrestrial N isotopic ratios (Fig. 3b). Three OR1f grains have ^{14}N excesses; grain OR1g1m-33 has the highest $^{14}N/^{15}N$ ratio (~1440) of any grain in this study; and three grains from OR1i are enriched in ^{14}N. Only three OR1f grains have ^{15}N enrichments. This lack of a large range of anomalies in nitrogen (Fig. 3a and b) has been previously observed in Murchison graphite as well (Hoppe et al., 1995). Because all theoretical models predict large C anomalies to be accompanied by large N anomalies, whatever the stellar source, the close-to-normal N isotopic ratios in most graphite grains were attributed to isotopic exchange or dilution of the original nitrogen, either on the parent body or during chemical processing in the laboratory. In view of the recent N ratio measurements on Genesis samples (Marty et al., 2011), it is interesting to note that HD graphite grains cluster around the terrestrial value of 272 and not the newly measured solar value of 459. This is an indication of equilibration/contamination with isotopically normal N in the solar nebula, parent body and/or the laboratory. Stadermann et al. (2005) found isotopic gradients in $^{12}C/^{13}C$ and $^{16}O/^{18}O$ ratios in ultramicrotome sections of a LD, Murchison KE3 graphite grain. The grain was found to be isotopically most anomalous at the center. No such gradients were found in the $^{14}N/^{15}N$ ratios. Oxygen isotopic gradients were attributed to isotopic exchange with isotopically normal material in the laboratory or on the parent body. Gradients in $^{12}C/^{13}C$ ratios can be explained by considering a grain growth environment where the C isotopic ratio varies during grain formation.

3.1.3. Oxygen isotopes

McKeegan et al. (2011) measured the solar $^{16}O/^{18}O$ ratio in Genesis solar wind material to be ~530. Similar to the case with N isotopes, we use the terrestrial value of 499 in this study to enable easy comparison with Murchison graphite data.

Fig. 4a and b show the $^{16}O/^{18}O$ ratios as a function of $^{12}C/^{13}C$ ratios for all the LD and HD fractions, respectively. One out of 7 grains in OR1c has a substantial ^{18}O excess (the $^{18}O/^{16}O$ ratio is ~4 times the solar value). It also exhibits a ^{15}N excess. Twenty-nine percent of the OR1d grains exhibit ^{18}O excesses, with $^{18}O/^{16}O$ ratios ranging up to 30 times the solar value of 0.002. More than 80% of the ^{18}O-enriched grains from this density fraction are also enriched in ^{15}N. The contaminated OR1d3m mount was the exception where only 2 out of 8 grains with isotopically heavy O also have ^{15}N excesses. Thus, 89% of grains with heavy O also contain isotopically heavy N. These ^{18}O-enriched grains show both depletion and enrichment in ^{13}C with respect to the solar value (Fig. 4a) and there does not seem to be any obvious correlation between the $^{12}C/^{13}C$ and $^{16}O/^{18}O$ ratios. Five ^{18}O-enriched grains have close-to-solar $^{12}C/^{13}C$ ratios (between 80 and 100).

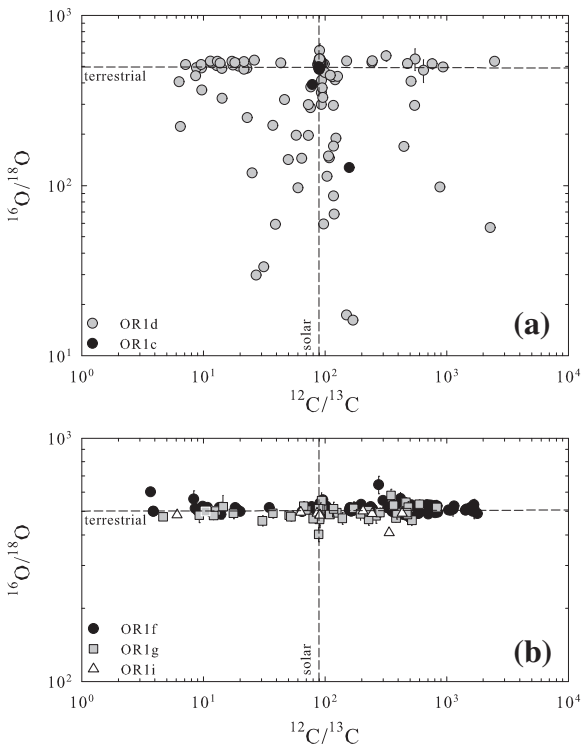

Fig. 4. (a) Carbon and oxygen isotopic ratios of LD graphites from the OR1c and OR1d fractions. (b) $^{12}C/^{13}C$ and $^{16}O/^{18}O$ ratios of HD graphites from the OR1f, OR1g and OR1i fractions. Dashed lines denote normal isotopic ratios ($^{12}C/^{13}C$ ~89; $^{16}O/^{18}O$ ~499). Error bars are 1σ.

Like N anomalies, O anomalies seem to disappear with increasing density. All the grains in the HD fractions, OR1f, 1g, and 1i, have $^{16}O/^{18}O$ ratios close to the solar value of 499 (Fig. 4b). Again, the most likely reason is equilibration/contamination with O of isotopically normal composition.

3.1.4. Silicon isotopes

The silicon isotopes, ^{28}Si, ^{29}Si, and ^{30}Si, were measured in grains from all the fractions. Fig. 5a and b show the results of these measurements as three-isotope δ-value plots. In general, grains in the LD fraction OR1d are dominated by ^{28}Si excesses, while HD grains (OR1f, 1g, and 1i) have ^{29}Si and ^{30}Si excesses.

The graphite grains in the density fraction OR1c were found to contain mostly isotopically normal Si (within errors; Fig. 5a). Among the analyzed grains from the other LD fraction, OR1d, approximately 20 grains have large ^{28}Si excesses (Fig. 5a). All the grains with ^{28}Si excesses are enriched in ^{18}O and/or also have ^{15}N excesses. Grain OR1d4m-1 has $\delta^{29}Si = -451 \pm 5‰$ and $\delta^{30}Si = -660 \pm 5‰$, the largest ^{28}Si enrichment seen in any Orgueil graphite grain. Some grains from the LD OR1d fraction are enriched in ^{29}Si or ^{30}Si. Grains OR1d4m-3 and OR1d1m-26 have a normal $^{29}Si/^{28}Si$ ratio but have a large ^{30}Si depletion ($\delta^{30}Si = -261 \pm 20‰$ and $-257 \pm 39‰$, respectively). OR1d1m-26 is also enriched in ^{18}O ($^{16}O/^{18}O$ ~409) and ^{15}N ($^{14}N/^{15}N$ ~160). Grains OR1d4m-18 and OR1d3m-5 are slightly depleted in ^{29}Si ($\delta^{29}Si = -80 \pm 14‰$ and $-64 \pm 21‰$, respectively) and enriched in ^{30}Si ($\delta^{30}Si = 84 \pm 20‰$ and $136 \pm 28‰$, respectively). Three grains, OR1d1m-17, OR1d1m-31, and OR1d3m-24, are enriched in ^{29}Si and depleted in ^{30}Si. They are also enriched in ^{18}O and ^{15}N. Grain OR1d1m-11 has a ^{30}Si excess and ^{29}Si deficit. It is also enriched in ^{18}O and ^{15}N, and contains isotopically heavy carbon ($^{12}C/^{13}C$ ~6).

The Si isotopic anomalies observed in grains from mount OR1d3m were not as large as those observed in the previous mounts of the same density fraction. They were apparently diluted due to contamination from the gold coat that was deposited on the mount prior to measurements. We only found four (out of 30) grains (OR1d3m-14, OR1d3m-16, OR1d3m-17, OR1d3m-18) on mount OR1d3m that contain ^{28}Si excesses. Not all of them contain ^{15}N or ^{18}O excesses; only one grain (OR1d3m-18) contains both. Because of the contamination, all Si isotopic anomalies in grains from this mount must be considered to be lower limits.

Fig. 5b shows Si isotopic ratios measured in grains from the heavy fractions OR1f, 1g and 1i. Grain OR1f2m-o67 is enriched in ^{30}Si and depleted in ^{29}Si. This grain is also highly enriched in ^{15}N. Two grains have extremely large ^{29}Si and ^{30}Si excesses: grain OR1f2m-o68 has $\delta^{29}Si = 1340 \pm 35‰$ and $\delta^{30}Si = 896 \pm 33‰$, and OR1f2m-o70 has $\delta^{29}Si = 1040 \pm 34‰$ and $\delta^{30}Si = 916 \pm 36‰$. Grains OR1f1m-16, OR1f1m-36, OR1f1m-34 and OR1f2m-o32 have smaller, but still large $\delta^{30}Si$ and $\delta^{29}Si$ values (Fig. 5b). More than 50% of grains from the three high-density fractions OR1f, 1g, and 1i are enriched in ^{30}Si and ^{29}Si. Grain OR1i1m-4 from the heaviest fraction has a large ^{28}Si excess. This grain is enriched in ^{14}N ($^{14}N/^{15}N$ ~475) and slightly enriched in ^{18}O ($^{16}O/^{18}O$ ~409), compared to terrestrial values.

Most of the grains (~75%) on the OR1f2m high-density mount have small anomalies or have normal $\delta^{29,30}Si/^{28}Si$ values (Fig. 5b). It is possible that the equilibration processes that cause the dilution of the N and O isotopic ratios also influence the Si isotopes.

Thus, the silicon isotopic data indicate distinctive trends that depend on the density of the grains, similar to the C, N, and O isotopes. While the LD fractions have mostly ^{28}Si-rich grains, the HD fractions have grains that are enriched in ^{30}Si and ^{29}Si. In general, most ^{30}Si-rich grains from the HD fractions contain isotopically light carbon (Fig. 6).

3.1.5. Al–Mg isotopes

On the initial mounts, OR1(d,f)1m, on which we measured Al–Mg isotopes, the graphite grains were embedded in macromolecular carbon and not on a separate mount (see Section 2.3). Thus, the Al–Mg measurements on the OR1(d,f)1m mounts are contaminated by ion signals from the surrounding macromolecular carbon and no ^{26}Mg excesses were detected in grains on these mounts.

Magnesium isotope results for the LD fraction OR1d are plotted as δ-values in Fig. 7a–d with different ranges of the plot axes to accommodate all the data. Fig. 8 shows Mg isotopic ratios for the grains from the HD fractions.

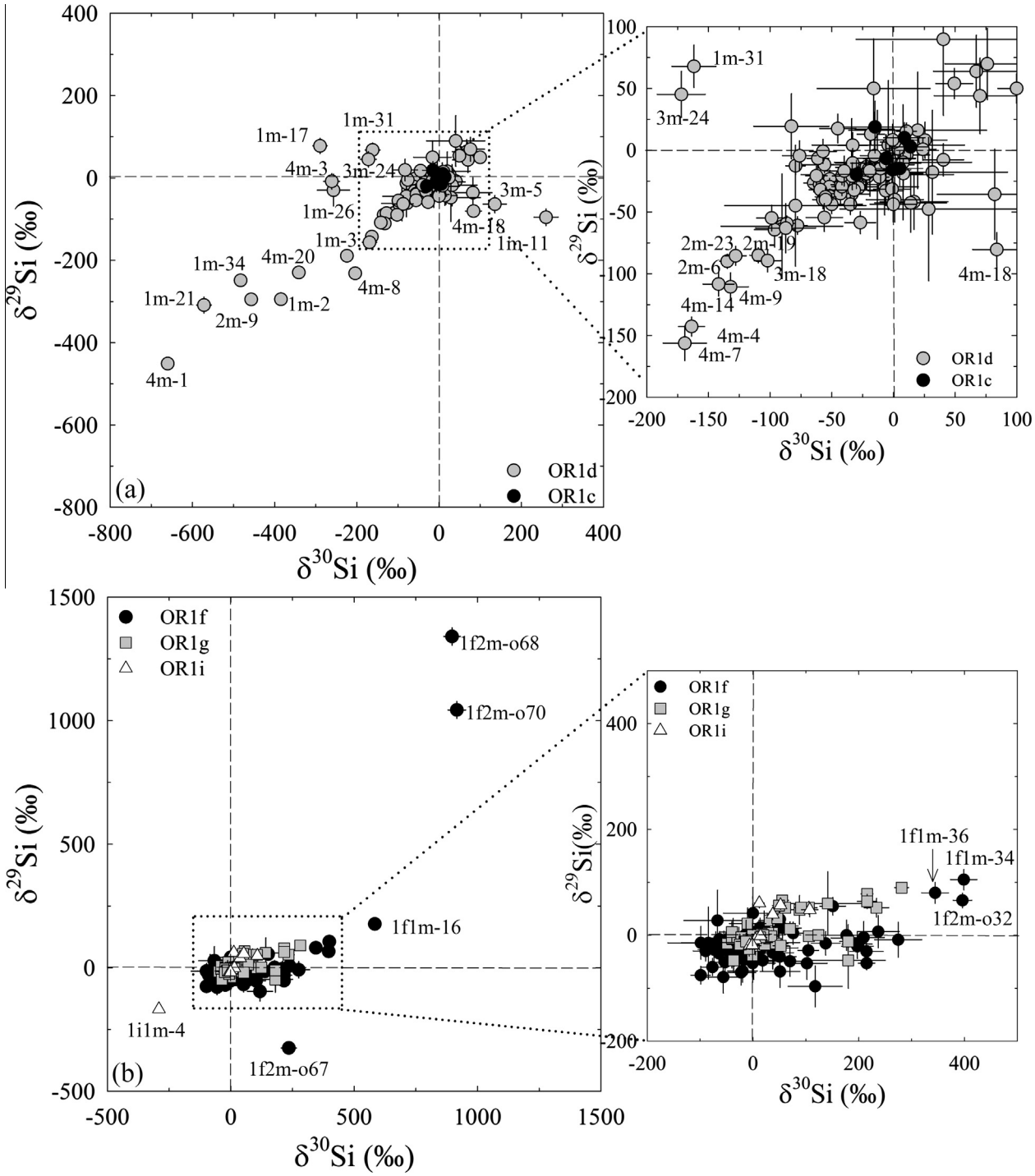

Fig. 5. Three-isotope plots of the Si ratios measured in graphite grains from (a) LD and (b) HD fractions. The ratios are plotted as δ-values, deviations from the terrestrial ratios in permil (‰). Error bars are 1σ. Dashed lines indicate the solar ratios ($\delta^{29}Si/^{28}Si = \delta^{30}Si/^{28}Si = 0$).

Fig. 9 displays the inferred $^{26}Al/^{27}Al$ ratios as a function of $^{12}C/^{13}C$ ratios for both the LD and HD grains with substantial ^{26}Mg excesses from the decay of short-lived ^{26}Al.

Fig. 7a is a plot of grains with the largest $\delta^{25}Mg$ and $\delta^{26}Mg$ values. Grain OR1d4m-20 has the largest inferred $^{26}Al/^{27}Al$ ratio (0.69 ± 0.06) seen in any presolar graphite grain so far. Such high $^{26}Al/^{27}Al$ ratios are found in SiC X grains (Nittler, 1996; Hoppe et al., 2000). The largest inferred $^{26}Al/^{27}Al$ ratio previously obtained in a Murchison KE3 graphite is ~0.146 (Travaglio et al., 1999). The grains labeled in Fig. 7a have large $^{26}Al/^{27}Al$ ratios (Fig. 9) and are enriched in ^{18}O and ^{28}Si. Except grain OR1d2m-32, all of these grains also have ^{15}N excesses. Interestingly, three grains (OR1d2m-19, OR1d4m-32, OR1d4m-20) have low

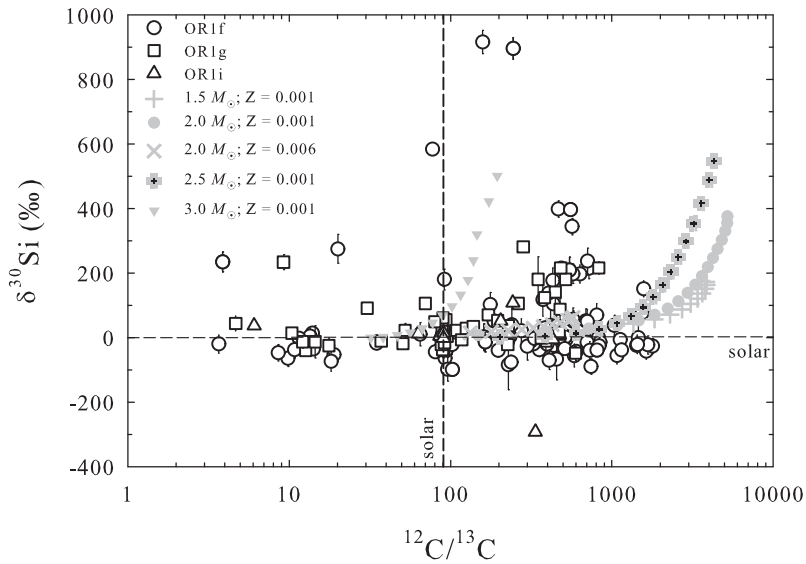

Fig. 6. The $\delta^{30}Si/^{28}Si$ values of graphite grains from the HD fractions OR1f, 1g and 1i are plotted against their $^{12}C/^{13}C$ ratios. These isotopic ratios are compared to model predictions of low-metallicity AGB stars from the F.R.U.I.T.Y. database (Cristallo et al., 2011). The dashed lines indicate solar values, and error bars are 1σ.

$^{12}C/^{13}C$ ratios, one is moderately ^{13}C-enriched, and two have roughly solar $^{12}C/^{13}C$ ratios. In general, grains from the OR1d2m and 4m mounts have the largest ^{26}Mg excesses (Fig. 7a–c). The inferred $^{26}Al/^{27}Al$ ratios range from 2×10^{-4} to 0.7 in these grains (Fig. 9). The high $^{26}Al/^{27}Al$ ratios we found in these grains were not seen in the study of grains from the OR1d1m and 3m mounts, most likely because of contamination present on those mounts, the first from the macromolecular carbon, and the second from the gold coating. The range of $^{26}Al/^{27}Al$ ratios in grains on mount OR1d1m is 2.5×10^{-4} to 0.04 and OR1d3m is 10^{-3} to 0.04. Only upper limits could be obtained for the inferred $^{26}Al/^{27}Al$ ratios for some of the grains with large errors associated with their measurements (Fig. 9).

In the HD fraction OR1f we found only one grain with high $^{26}Al/^{27}Al$ ratio. Grain OR1f2m-o67 has the largest ^{26}Mg excess ($\delta^{26}Mg = 1590‰$) (Fig. 8) and an inferred $^{26}Al/^{27}Al$ ratio of 0.01 (Fig. 9). Three other grains (OR1f2m-25, OR1f2m-38, OR1f2m-o8) have inferred $^{26}Al/^{27}Al$ ratios on the order of 10^{-4}. The two grains with the highest $^{26}Al/^{27}Al$ ratios are highly enriched in ^{13}C (Fig. 9) while the other two grains are ^{12}C-enriched.

The Al/Mg ratios in the grains of this fraction were very low, making the detection of any ^{26}Mg excesses from the decay of radiogenic ^{26}Al very challenging. There is a possibility that the equilibration processes affecting the N and O in HD graphite grains also introduced normal Mg (this would explain low Al/Mg ratios) and diluted the Mg isotopic ratios in these grains. It is also interesting to note that grains OR1f2m-o67 and OR1f2m-o8 were measured for Mg isotopes when they were on mount OR1f1m and the surrounding material made it impossible to detect any large ^{26}Mg excesses in these grains. Excesses were measureable only after remounting the grains.

3.1.6. K isotopes

Most grains from the LD fraction OR1d were found to have normal $^{41}K/^{39}K$ ratios (solar value ~0.072), but four grains have $^{41}K/^{39}K$ ratios ranging from 0.074 to 0.106. These ^{41}K excesses can be attributed to the decay of ^{41}Ca ($\tau_{1/2} = 1.03 \times 10^5$ a) because the intrinsic concentration of K in graphite grains is expected to be very low (Amari et al., 1996). The inferred $^{41}Ca/^{40}Ca$ ratios for these grains range from 0.008 to 0.015 (Fig. 10; Appendix Table A2). All grains with high $^{41}Ca/^{40}Ca$ ratios have ^{18}O excesses and high $^{26}Al/^{27}Al$ ratios. Two of them are also enriched in ^{28}Si.

The LD mount OR1d3m was found to be contaminated by large amounts of terrestrial K and Ca, making the detection of radiogenic ^{41}Ca nearly impossible.

Most of the grains from the HD fraction OR1f have normal $^{41}K/^{39}K$ ratios (0.072). Only three grains have elevated $^{41}K/^{39}K$ ratios ranging from 0.09 to 1.00. The inferred $^{41}Ca/^{40}Ca$ ratios range up to 0.01 (Fig. 10; Appendix Table A2).

3.1.7. Ca isotopes

The Ca isotopic ratios of LD grains plotted in Fig. 11a–c and those with significant anomalies are listed in Appendix Table A3. Grains on mount OR1d3m were affected by the Ca contamination and have normal Ca isotopic ratios (within errors); only one grain (OR1d3m-5) has a high $\delta^{44}Ca/^{40}Ca$ value of $222 \pm 22‰$ and a comparable excess in ^{43}Ca ($\delta^{43}Ca/^{40}Ca = 154 \pm 43‰$). Since these excesses are of approximately the same magnitude, they can be explained by neutron capture and the ^{44}Ca excess does not constitute evidence for the presence of ^{44}Ti.

Four LD graphite grains (OR1d4m-3, OR1d4m-10, OR1d4m-16, and OR1d4m-20) from the other LD mount, OR1d4m, were found to have high $\delta^{42,43,44}Ca/^{40}Ca$ values that appear to be correlated (Fig. 11a and b). Three grains

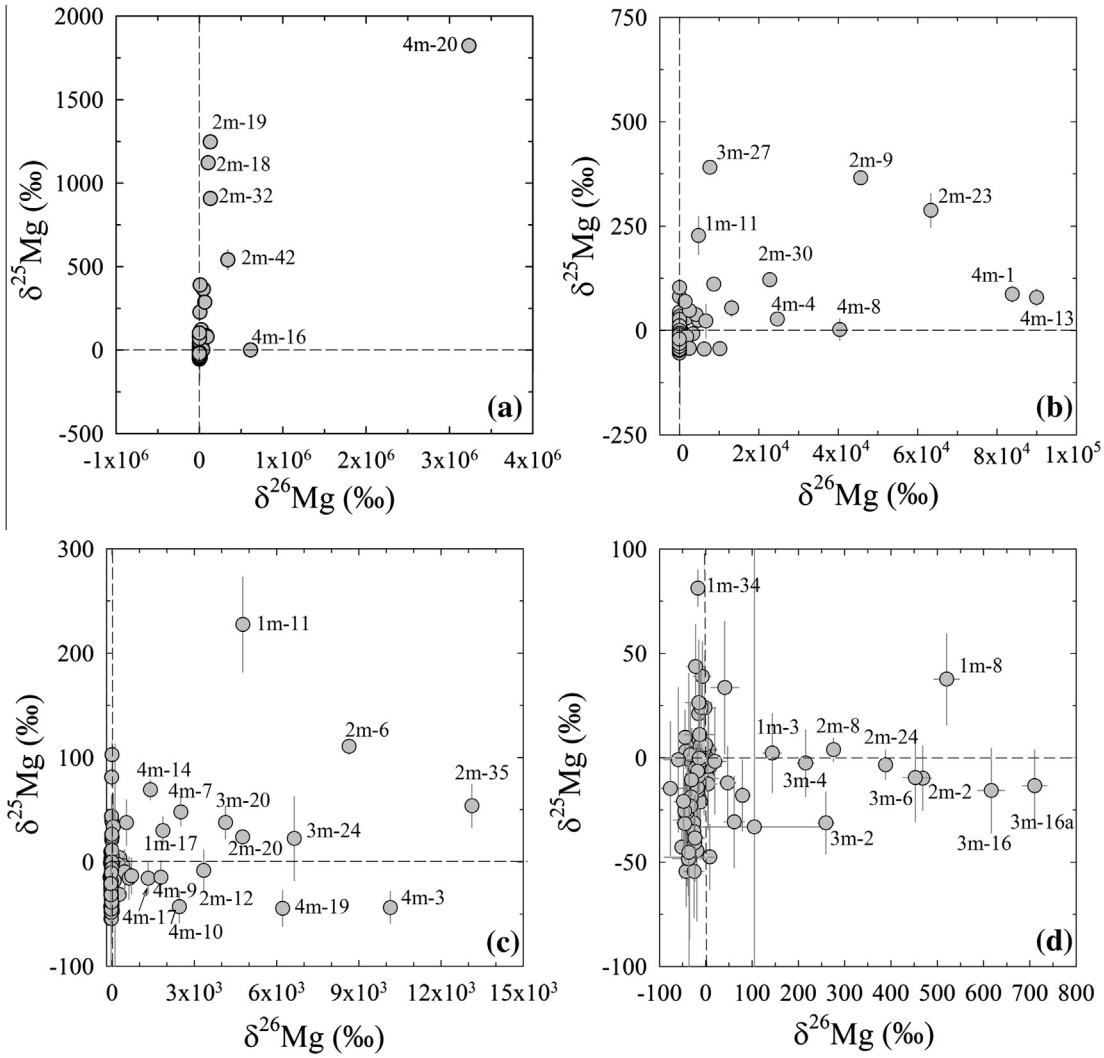

Fig. 7. Three-isotope plots of the Mg ratios measured in graphite grains from the LD fraction OR1d. The ratios are plotted as δ-values, deviations from the terrestrial ratios in permil (‰). Error bars are 1σ. Dashed lines indicate solar ratios ($\delta^{25}Mg/^{24}Mg = \delta^{26}Mg/^{24}Mg = 0$). Each progressive Fig. numbered with letters (b), (c) and (d) represents a magnified area around the origin of the previous plot.

(OR1d4m-8, OR1d4m-9, and OR1d4m-19) contain large ^{44}Ca excesses that are much larger than their ^{42,43}Ca/^{40}Ca excesses. Slow neutron capture that gives rise to ^{44}Ca excesses is expected to produce even larger ^{42,43}Ca excesses and hence, we conclude that the ^{44}Ca excesses in OR1d4m-8 and OR1d4m-9 must be due to the decay of ^{44}Ti. The inferred initial ^{44}Ti/^{48}Ti ratios in these two grains are listed in Appendix Tables A3 and A4. Higher values, up to ~0.6, have been observed in SiC X grains (Amari et al., 1992; Hoppe et al., 1996, 2000; Nittler et al., 1996; Besmehn and Hoppe, 2003; Lin et al., 2010) and KE3 graphites from Murchison (Travaglio et al., 1999).

Table 2 lists the C, Ca and Ti isotopic ratios of interesting grains from the HD fraction OR1f. Fig. 12a and b show that several grains from this fraction have unusually large $\delta^{42,43,44}$Ca values. Grains OR1f2m-9, OR1f2m-18, OR1f2m-29, OR1f2m-34, OR1f2m-40, and OR1f2m-o68 exhibit extremely large ^{42,43}Ca excesses and comparable or smaller ^{44}Ca excesses. In grains OR1f2m-1, OR1f2m-25, OR1f2m-38, and OR1f2m-o67 the large ^{44}Ca excesses must be the result of the decay of ^{44}Ti. Table 2 and Appendix Table A4 list the inferred ^{44}Ti values for these grains. During NanoSIMS analysis of the grains, ion signals clearly show a correlation of the ^{44}Ca ion signal with the ^{48}Ti ion signal. The fact that the ^{44}Ca signal does not correlate with any other Ca ion signals is additional evidence that ^{44}Ca excesses are of radiogenic origin. Three of the four grains from OR1f with ^{44}Ti excesses have ^{12}C/^{13}C ratios less than 20 (Table 2). OR1f2m-25 is the only grain with both ^{44}Ti and ^{12}C excesses (^{12}C/^{13}C ~743). Approximately half the grains with large Ca isotopic anomalies, listed in Table 2, are enriched in ^{13}C while the others are enriched in ^{12}C.

3.1.8. Ti isotopes

Fig. 13a–c display the Ti isotopic ratios of the grains from the LD fraction OR1d. Grain OR1d4m-13 has a large excess in ^{47}Ti without any accompanying ^{46}Ti excess, and

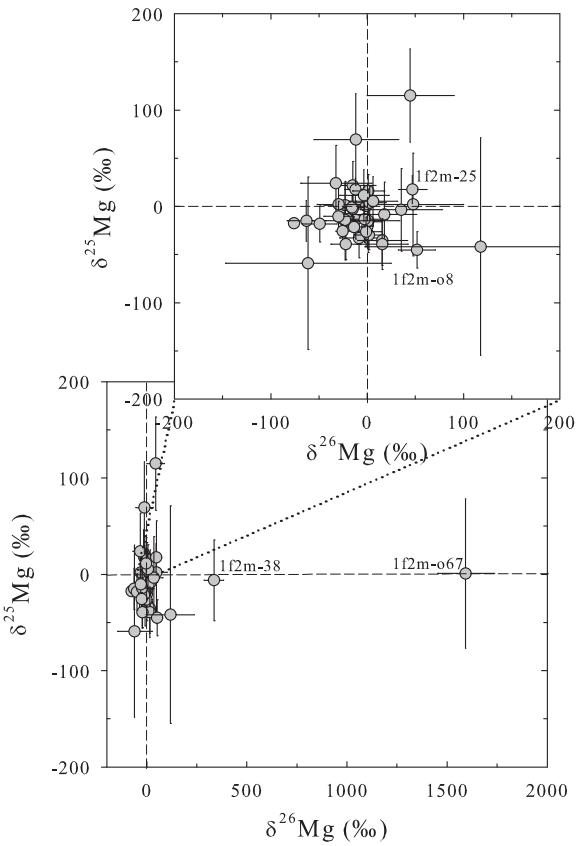

Fig. 8. Three-isotope plots of the Mg ratios measured in graphite grains from the HD fraction OR1f. The ratios are plotted as δ-values, deviations from the terrestrial ratios in permil (‰). Error bars are 1σ. Dashed lines indicate solar ratios ($\delta^{25}Mg/^{24}Mg = \delta^{26}Mg/^{24}Mg = 0$).

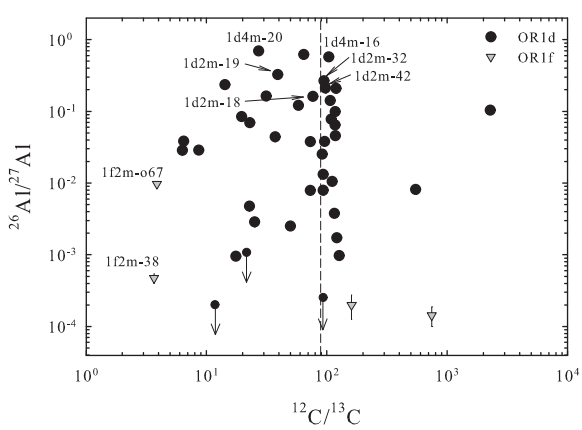

Fig. 9. Inferred $^{26}Al/^{27}Al$ ratios from ^{26}Mg excesses for LD and HD grains plotted versus $^{12}C/^{13}C$ ratios. The symbols with arrows represent 1σ upper limits for grains with large error bars. Error bars are 1σ. The dashed line indicates the solar $^{12}C/^{13}C$ ratio.

grains OR1d4m-9, OR1d4m-14 and OR1d4m-19 are significantly depleted in $^{46,47}Ti$. Several grains have correlated excesses in $^{46,47}Ti$ (within errors). Eight grains are highly enriched ($\delta^{49}Ti > 500‰$) in ^{49}Ti (as high as $1600 \pm 85‰$

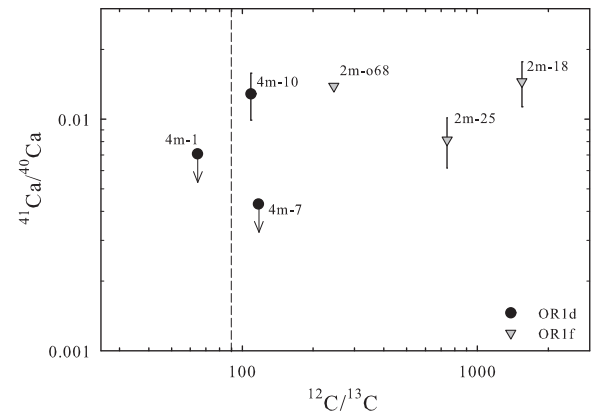

Fig. 10. Inferred $^{41}Ca/^{40}Ca$ ratios from ^{41}K excesses for LD (circles) grains and HD (triangle) grains plotted versus $^{12}C/^{13}C$ ratios. The ratios are listed in Appendix Table A2. The symbols with arrows represent 1σ upper limits for grains with large error bars. Error bars are 1σ. The dashed line indicates the solar $^{12}C/^{13}C$ ratio.

in grain OR1d3m-2; Appendix Table A3), while seven grains have moderate excesses ($\delta^{49}Ti < 500‰$, Fig. 13b). Due to a very high ^{50}Cr signal (inferred from ^{52}Cr) that interfered with ^{50}Ti, we were unable to obtain good ^{50}Ti data on a majority of the grains. The grains acquire Cr from $Na_2Cr_2O_7$, which is used as an oxidizing agent to remove macromolecular carbon during chemical separation in the laboratory. Four grains that have less than a 60% ^{50}Cr contribution to their ^{50}Ti ion signal have elevated $\delta^{50}Ti/^{48}Ti$ values (Fig. 13c). Most of the grains in this LD fraction that have Ti anomalies have ^{18}O, ^{15}N, ^{28}Si excesses, and high $^{26}Al/^{27}Al$ ratios.

Some of the grains from the HD fraction OR1f have extremely large $^{46,47,49,50}Ti$ excesses, similar to the $^{42,43,44}Ca$ excesses (Fig. 14a–c; Table 2). The largest of these are seen in OR1f2m-9 ($\delta^{46}Ti = 35030 \pm 4430‰$; $\delta^{47}Ti = 1380 \pm 371‰$; $\delta^{49}Ti = 2280 \pm 298‰$; $\delta^{50}Ti = 32830 \pm 4590‰$. The other grains, some with similarly large anomalies, are listed in Table 2 in addition to the other interesting grains from the HD fraction.

3.1.9. Summary of isotopic compositions

In summary, we find that the presolar graphites from Orgueil tend to have C, N, O, Al–Mg, and Si isotopic properties that are density dependent. Many LD grains have ^{15}N, ^{18}O, ^{28}Si excesses and high $^{26}Al/^{27}Al$ ratios. Most HD grains have terrestrial N and O isotopic ratios, contain ^{29}Si and ^{30}Si excesses that correlate with ^{12}C excesses, and have smaller $^{26}Al/^{27}Al$ ratios than LD grains. The original N and O isotopic ratios in the HD fractions are assumed to be diluted by normal N and O. It is possible that the equilibration processes affecting the N and O ratios also dilute the Si and Mg isotopic signatures in the HD grains. However, these processes apparently spared the Ca and Ti isotopic ratios in these grains. Some of the HD grains have extreme anomalies in Ca and Ti while their Si and Al–Mg anomalies are negligible in comparison. The *s*-process neutron capture reactions that cause excesses in Ca and Ti

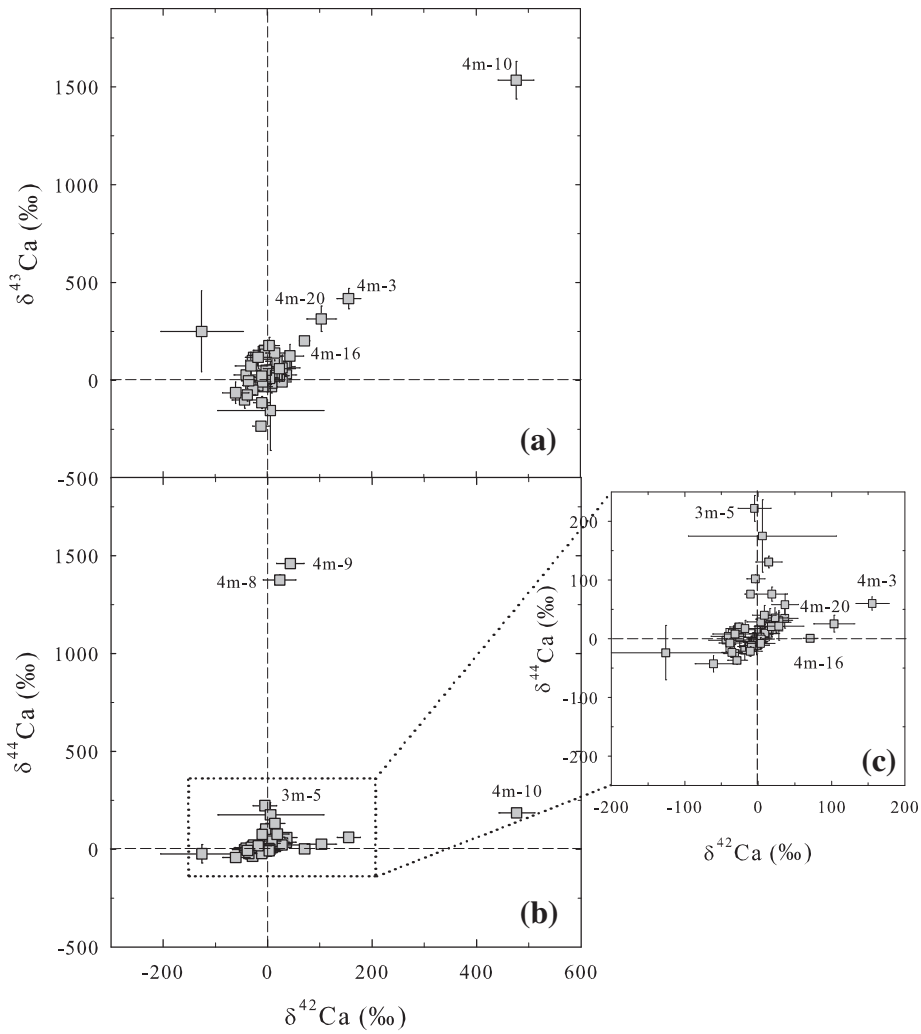

Fig. 11. Delta-value three-isotope plots of the Ca isotopic ratios measured in graphite grains from the LD fraction OR1d. Grains with large delta values are listed in Appendix Table A3. The ratios are plotted as δ-values, deviations from the terrestrial ratios in permil (‰). Error bars are 1σ. Dashed lines indicate solar ratios.

isotopes should have caused significant Mg and Si anomalies as well. Titanium is observed in subgrains and hence, tougher to equilibrate compared to the other elements like Si and Mg, which are uniformly distributed throughout the host grain. It is possible that Ca had a higher abundance in HD grains compared to Si and Mg and, being more refractory was not completely equilibrated. Low-density grains do not exhibit similar extreme anomalies in Ca and Ti.

4. DISCUSSION – STELLAR SOURCES OF ORGUEIL GRAPHITES

Presolar dust grains condensed in cooling atmospheres of dying stars, either in the ejecta of stellar explosions or in the outflows from late-type stars. There is an additional constraint for the condensation of C-rich dust grains: under thermodynamic equilibrium, the carbon content in the gas should be greater than the oxygen content, i.e., C/O > 1 (Larimer, 1975; Lodders and Fegley, 1995; Sharp and Wasserburg, 1995). We will present arguments against the scenario of grains condensing in C < O environments suggested by Clayton et al. (1999), Clayton (2011), and Deneault et al. (2003, 2006) in the next section. The C > O condition can be satisfied at various stellar sites. The envelopes or the interior layers of carbon stars or AGB stars, Wolf–Rayet stars, novae, and different Type II SN zones all satisfy this condition at some time in their lifecycles. The C > O condition is expected to be unachievable in Type Ia SNe ejecta (Nomoto et al., 1984; Thielemann et al., 1986; Woosley et al., 1986) and the grain data do not agree with the isotopic ratios produced by He burning in such SNe. Thus, we only refer to Type II SNe as one of the possible stellar sources for the putative SN grains discussed in this paper.

Presolar graphite grains can have several stellar sources, which are revealed by their complex isotopic compositions. In this section, we discuss the various stellar sources of presolar graphite grains from Orgueil.

Table 2
C, Ca and Ti isotopic ratios of HD graphite grains from OR1f.

Grain	$^{12}C/^{13}C$	$^{41}Ca/^{40}Ca$	$\delta^{42}Ca/^{40}Ca$ (‰)	$\delta^{43}Ca/^{40}Ca$ (‰)	$\delta^{44}Ca/^{40}Ca$ (‰)	$^{44}Ti/^{48}Ti$ ($\times 10^{-3}$)	$\delta^{46}Ti/^{48}Ti$ (‰)	$\delta^{47}Ti/^{48}Ti$ (‰)	$\delta^{49}Ti/^{48}Ti$ (‰)	$\delta^{50}Ti/^{48}Ti$ (‰)
OR1f2m-1	14	[a]	−152 ± 96	156 ± 239	6018 ± 203	0.44 ± 0.01	−15 ± 8	−28 ± 9	161 ± 11	44 ± 15
OR1f2m-9	18	[a]	16030 ± 316	27640 ± 805	9400 ± 151	[c]	35030 ± 4430	1380 ± 371	2280 ± 298	32830 ± 4590
OR1f2m-13	836	[a]	77 ± 48	142 ± 104	157 ± 30	[c]	613 ± 116	318 ± 129	966 ± 209	[b]
OR1f2m-18	1545	0.015 ± 0.003	992 ± 58	4060 ± 201	2040 ± 46	[c]	522 ± 98	2120 ± 354	2650 ± 204	[b]
OR1f2m-21	472	[a]	−42 ± 46	48 ± 103	−13 ± 28	[c]	387 ± 66	80 ± 59	679 ± 123	1722 ± 337
OR1f2m-22	94	[a]	−7 ± 4	6 ± 8	5 ± 2	[c]	446 ± 31	413 ± 32	482 ± 39	472 ± 46
OR1f2m-25	743	0.008 ± 0.002	93 ± 22	90 ± 42	1584 ± 26	2.38 ± 0.04	58 ± 5	−32 ± 12	754 ± 20	214 ± 23
OR1f2m-29	10	[a]	1450 ± 50	1630 ± 100	540 ± 24	[c]	[d]	[d]	[d]	[d]
OR1f2m-33	574	[a]	−5 ± 58	9 ± 122	104 ± 37	[c]	477 ± 24	97 ± 27	1237 ± 38	2621 ± 296
OR1f2m-34	9	[a]	5060 ± 60	7410 ± 146	2180 ± 25	[c]	[d]	[d]	[d]	[d]
OR1f2m-38	4	[a]	−118 ± 177	−602 ± 274	51890 ± 1500	1.84 ± 0.05	−77 ± 12	−98 ± 15	125 ± 6	242 ± 6
OR1f2m-39	332	[a]	21 ± 38	−30 ± 79	-19 ± 22	[c]	285 ± 100	78 ± 79	614 ± 64	4224 ± 1568
OR1f2m-40	11	[a]	3380 ± 65	3660 ± 138	554 ± 22	[c]	[d]	[d]	[d]	[d]
OR1f2m-o65	546	[a]	340 ± 120	294 ± 252	26 ± 63	[c]	1180 ± 30	310 ± 20	1800 ± 37	7420 ± 154
OR1f2m-o67	4	[a]	63 ± 52	15 ± 107	3770 ± 77	1.77 ± 0.04	2 ± 4	14 ± 4	169 ± 5	236 ± 6
OR1f2m-o68	245	0.0139 ± 0.0001	996 ± 13	2840 ± 41	289 ± 7	[c]	1980 ± 160	327 ± 98	1560 ± 169	2180 ± 329

Note: Errors are 1σ; δ-values are deviations from solar ratios in per mil.

[a] The Ca/K ratios for these grains were very low, making it impossible to derive a meaningful $^{41}Ca/^{40}Ca$ ratio from the ^{41}K excess.

[b] Not reported, because the ^{50}Cr contribution to the ion signal of these grains was calculated to be ~60%, increasing the uncertainty of the results.

[c] Did not derive $^{44}Ti/^{48}Ti$ ratios for these grains because they either had no ^{44}Ca excess or the $d^{44}Ca/^{40}Ca$ values are comparable to the $d^{42,43}Ca/^{40}Ca$ values.

[d] Not measured because of very low Ti signals.

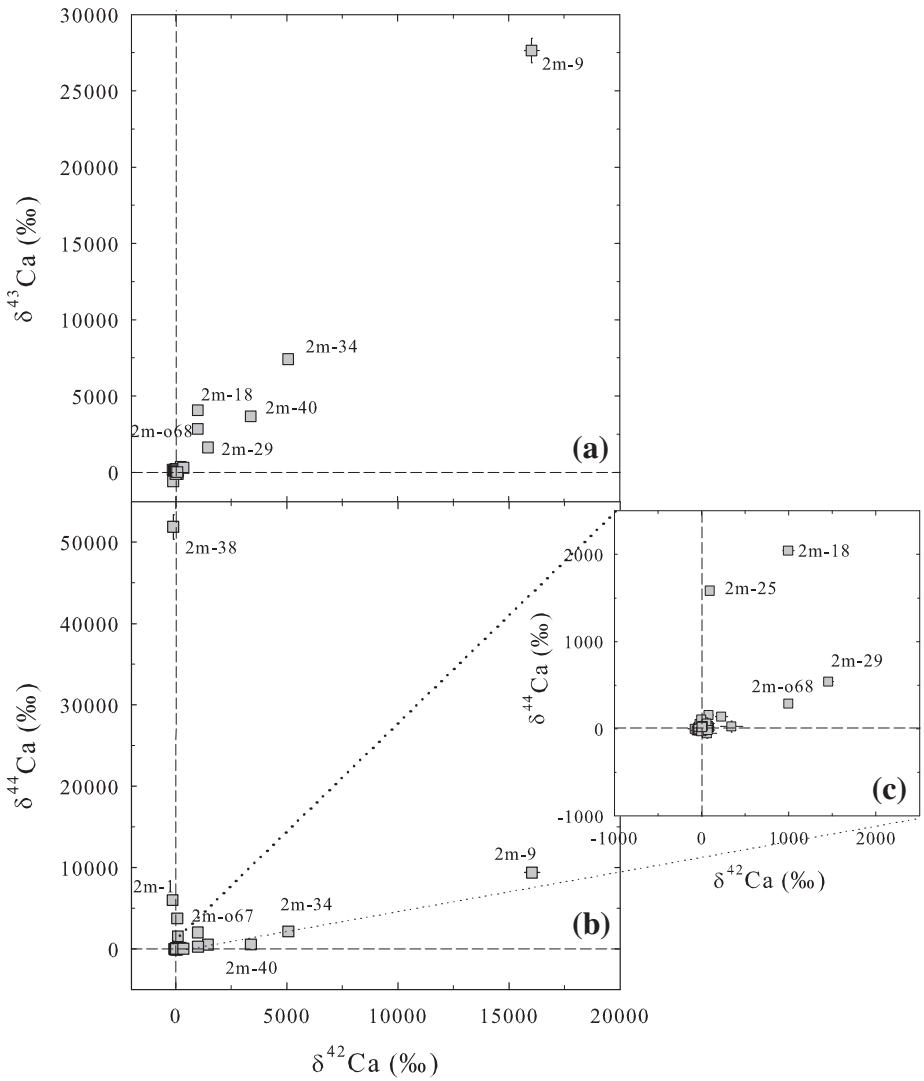

Fig. 12. Delta-value three-isotope plots of the Ca isotopic ratios measured in graphite grains from the HD fraction OR1f. Grains with extreme delta values are listed in Table 2. The ratios are plotted as δ-values, deviations from the terrestrial ratios in permil (‰). Error bars are 1σ. Dashed lines indicate solar ratios.

4.1. Orgueil graphites from supernovae

Several isotopic signatures indicate a SN origin for Orgueil graphite grains. They include excesses in ^{15}N, ^{18}O, ^{28}Si, high inferred ^{26}Al/^{27}Al ratios, and evidence for initial ^{44}Ti. The presence of several of these isotopic signatures in an individual grain requires that several different SN zones must have contributed material to the mixture from which the grain condensed. X-ray observations of SN remnants (SNRs) of Cassiopeia A (Hughes et al., 2000) and SN 1978A (Ebisuzaki and Shibazaki, 1988) indicate extensive mixing in SN ejecta. Furthermore, hydrodynamic models of SN explosions by Herant et al. (1994) have predicted that mixing of various SN layers can be initiated by Rayleigh–Taylor instabilities between the layers. The detailed mechanics of this mixing and whether it occurs on a microscopic level are still unclear. To date, several attempts have been made to match the isotopic ratios of graphite and SiC grains from supernovae by mixing of different SN zones (Travaglio et al., 1998; Yoshida and Hashimoto, 2004; Yoshida, 2007; Marhas et al., 2008; Fedkin et al., 2010; Lin et al., 2010). An attempt to explain the isotopic ratios of each SN grain of this study in detail would exceed the scope of the present paper. We, instead, discuss the problems and limitations that arise when one tries to match isotopic ratios of multiple elements of a given grain by mixing different SN layers. The labels given to different layers of a SN that we refer to in the rest of this paper follow the nomenclature introduced by Meyer et al. (1995) based on the most abundant elements present in each zone.

The first question to be addressed is whether a grain's isotopic composition measured in the laboratory is the same as that at the time of grain formation. We know that grains initially carried some short-lived isotopes that decayed during the grains' lifetime and we can determine their abundance from their daughter isotopes. Here we

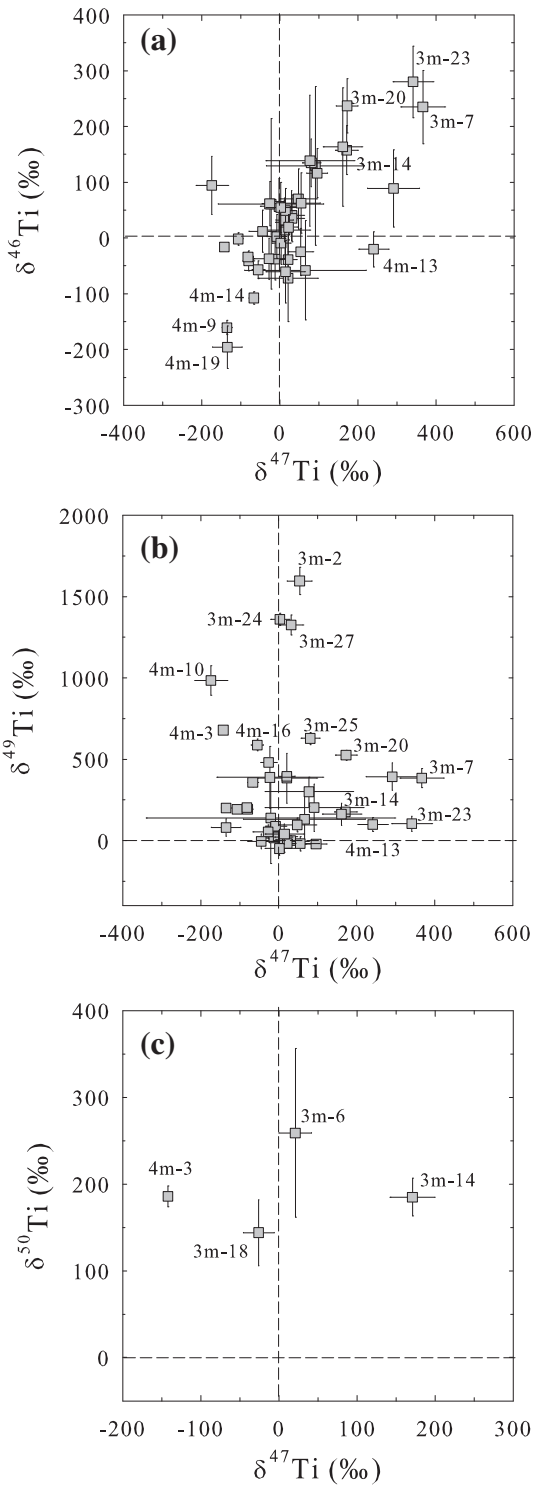

Fig. 13. Delta-value three-isotope plots of Ti isotopic ratios measured in graphite grains from the LD OR1d fraction. Grains with large delta values are listed in Appendix Table A3. The ratios are plotted as δ-values, deviations from the terrestrial ratios in permil (‰). Error bars are 1σ. Dashed lines indicate solar ratios.

are concerned with stable isotopes. The question of isotopic equilibration and contamination has been raised previously in connection with the N and O isotopic ratios of many presolar graphite grains. It is difficult to understand why many grains, especially HD grains, with a large range in their C isotopic ratios, have close-to-terrestrial N and O isotopic ratios (Figs. 3 and 4). Isotopic equilibration has been invoked to explain C and O isotopic heterogeneity observed in thin slices of a LD graphite grain from Murchison (Stadermann et al., 2005). On the other hand, contamination has also to be considered, especially for graphite grains from Orgueil, which could not be separated from macromolecular IOM by chemical processing. Groopman et al. (2012) observed large N and O isotopic variations in isotopic images of the surfaces of LD graphite grains from Orgueil and explained it by adhering IOM material. Such contamination could certainly be present in the present study, especially for grains that were not extracted from the IOM before NanoSIMS analysis. Another point of concern is intrinsic isotopic heterogeneity within grains. Groopman et al. (2012) interpreted isotopic heterogeneity in C, N, and O measured in thin slices of OR1d grains as being caused by changing isotopic compositions in the SN ejecta during grain growth. Stadermann et al. (2005) found internal TiC subgrains that have much larger ^{18}O excesses than the surrounding graphite host. Since the TiC grains must have formed before the host grain and were incorporated during its growth, it is conceivable that they formed in a different environment with different isotopic compositions. While internal variations revealed by isotopic imaging offers a fascinating way to study the history of the formation of a given grain, in the present study different isotopic systems were measured sequentially in different layers that were sputtered away by the primary beam (Appendix Table A1). If isotopic compositions changed because of intrinsic heterogeneity, we do not have coordinated isotopic compositions for a given sub-volume of the grain. Thus, we would like to point out that comparison of grain data with results of mixing calculations cannot provide an exact solution. Another reason why a unique solution is unrealistic is that despite large efforts made by SN modelers, SN models can at best only be considered as approximations. First, all models that provide the abundances of different nuclides are one-dimensional models (Woosley and Weaver, 1995; Thielemann et al., 1996; Rauscher et al., 2002; Limongi and Chieffi, 2003, 2006; Yoshida and Hashimoto, 2004). Two- and three-dimensional models of SN explosions have recently been computed (Müller et al., 1991; Kifonidis et al., 2003; Joggerst et al., 2009; Hammer et al., 2010), but these models did not follow the nucleosynthesis of a large network during the explosion. Second, SN models cannot explain certain isotopic ratios measured in the grains. For example, inferred ^{26}Al/^{27}Al ratios in some graphite grains (Fig. 9) and SiC grains of type X (Lin et al., 2010) are larger than the predictions of any existing SN models. Silicon isotopic ratios in X grains are another example of anomalies that cannot be successfully matched by SN models (Lin et al., 2010). Another complication for the comparison of grain data with SN models is the possibility of fractionation

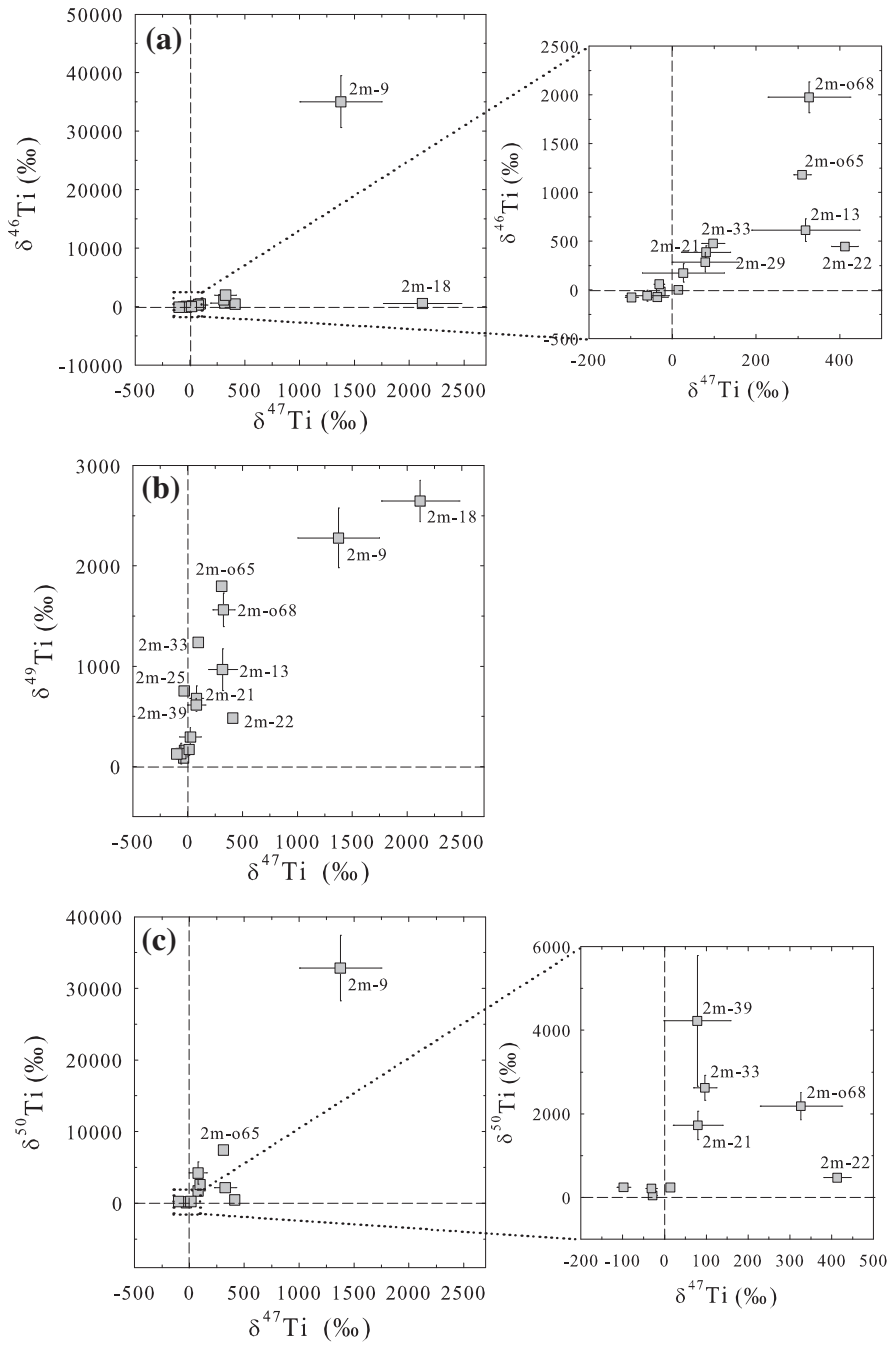

Fig. 14. Delta-value three-isotope plots of Ti isotopic ratios measured in graphite grains from the HD OR1f fraction. Grains with extreme delta values are listed in Table 2. The ratios are plotted as δ-values, deviations from the terrestrial ratios in permil (‰). Error bars are 1σ. Dashed lines indicate solar ratios.

between elements of a given SN zone. Usually, although different SN zones contributed different percentages to the mix from which a grain condensed, it is assumed that there is no elemental fractionation for a given zone. However, observations of presolar grains force us to conclude that this assumption is not warranted. A prime example of elemental fractionation are SiC type C grains, rare grains that appear to have a SN origin (Gyngard et al., 2010; Hoppe et al., 2010, 2012; Zinner et al., 2010). These grains have large excesses of ^{29}Si and ^{30}Si, and some have large ^{32}S excesses (Croat et al., 2010; Gyngard et al., 2010; Hoppe et al., 2010, 2012; Zinner et al., 2010; Xu et al., 2012). The Si/S SN zone contains almost pure ^{28}Si and ^{32}S, thus ^{32}S excesses are expected to be accompanied by large ^{28}Si excesses. Because this is not observed in SiC C grains, Si and S from the Si/S zone must have been fractionated from one another before grain formation (Hoppe et al.,

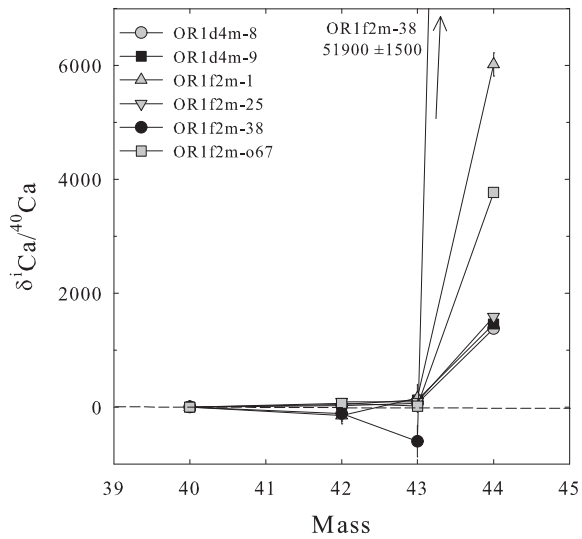

Fig. 15. Ca isotopic patterns observed in 6 graphite grains from the LD and HD fractions, OR1d and OR1f. All these grains have ^{44}Ca excesses that vastly exceed the ^{42,43}Ca excesses, seen in the grains, indicating the initial presence of the short-lived radionuclide ^{44}Ti. The derived ^{44}Ti/^{48}Ti ratios for these grains are listed in Appendix Table A4.

2012). Another example is the lack of ^{54}Fe excesses in SiC X grains (Marhas et al., 2008). The Si/S zone is rich in ^{54}Fe, which is expected to accompany ^{28}Si. Before the formation of these grains, Si and Fe from the Si/S zone must have been fractionated from one another, possibly by forming FeS molecules and grains.

It is with all these caveats that we compare the isotopic compositions of Orgueil graphite grains with theoretical predictions of SN models.

4.1.1. Bona fide supernova grains among the LD and HD density fractions

Definite evidence of a SN origin is obtained from the presence of ^{44}Ti and ^{28}Si excesses in graphite (or any presolar) grains. Both isotopes are only produced in massive stars (Timmes et al., 1996; see also Meyer and Zinner, 2006). Fig. 15 shows extremely large ^{44}Ca excesses in six grains, which show only small or no excesses in ^{42}Ca and ^{43}Ca. Two of these grains belong to the LD fraction, while the other four are from the HD fraction.

Almost all SiC X grains and LD graphite grains from Murchison that show evidence of ^{44}Ti have large ^{28}Si excesses (Amari et al., 1992; Hoppe et al., 1994, 1996, 2000; Nittler et al., 1996; Besmehn and Hoppe, 2003). In the present study, however, 3 out of 4 HD graphites that contain ^{44}Ti have only small if any ^{28}Si excesses (Fig. 16). The Si isotopic ratios of these grains are believed to be equilibrated similar to their N and O isotopic ratios. Grain OR1f2m-o67 is depleted in ^{29}Si and enriched in ^{30}Si, and hence does not have a ^{28}Si excess. The two LD grains, OR1d4m-8 and OR1d4m-9, contain both ^{44}Ti and large ^{28}Si excesses. In addition to these 2 LD grains, there are approximately 20 more LD grains that have large ^{28}Si excesses (Fig. 5a) but show no evidence for the initial presence of ^{44}Ti. The presence of ^{44}Ti and/or ^{28}Si excesses, however, indicates beyond any doubt that these grains originated in Type II SNe. To explain these ^{28}Si and ^{44}Ti anomalies, we need a contribution from the Si/S zone of a Type II SN. We discuss further issues related to this mixing in the following Section 4.1.2. It is now clear that grains from different stellar sources are found in LD and HD types of graphites, and SN grains are present in both types of Orgueil graphites. Zirconium and Mo isotopic analyses of HD graphites from Murchison (Nicolussi et al., 1998a) indicate a similar result. These authors found two grains with extreme ^{96}Zr excesses, which the authors interpret as a

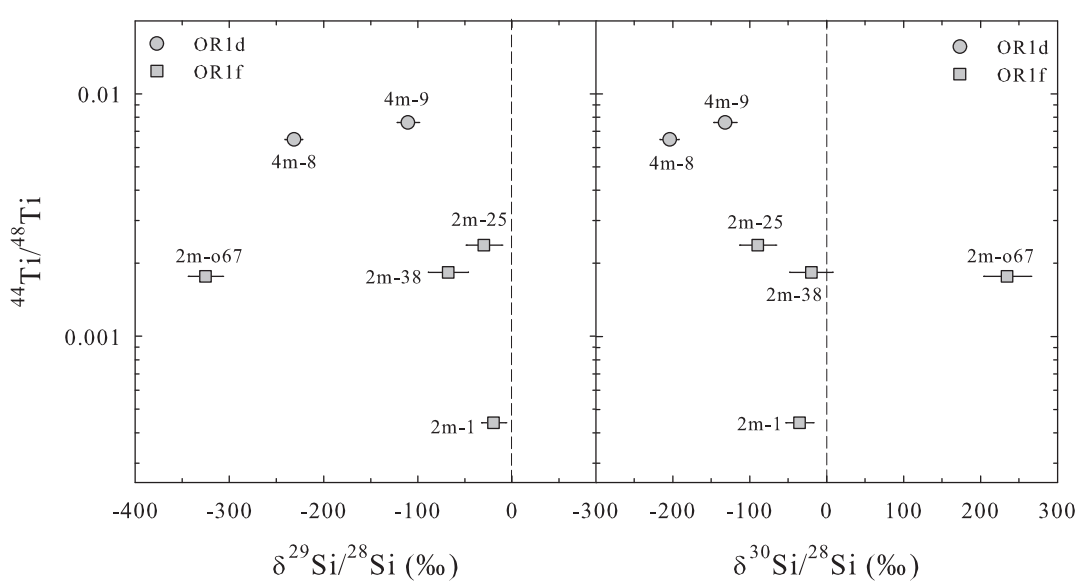

Fig. 16. Inferred ^{44}Ti/^{48}Ti ratios in graphite grains from both LD and HD fractions OR1d and OR1f are plotted as a function of Si isotopic ratios. Three out of the six graphites with high ^{44}Ti/^{48}Ti ratios do not have large ^{28}Si excesses.

signature of a SN origin for these HD grains. Several other grains showed *s*-process isotopic patterns for Zr and Mo, similar to mainstream SiC grains that come from AGB stars. However, it is possible for AGB stars with low-mass and metallicity to also produce large ^{96}Zr excesses (Davis et al., 2003) and this discrepancy could be resolved if other isotopic ratios were measured in the two SN grains reported by Nicolussi et al. (1998a). This illustrates the value of obtaining multi-element isotopic analyses on individual presolar grains.

The HD grains OR1f2m-1, OR1f2m-38, and OR1f2m-o67 with evidence for the initial presence of ^{44}Ti also have low ^{12}C/^{13}C ratios (<20). We will demonstrate in the next Section 4.1.2 that it is difficult to reconcile the low ^{12}C/^{13}C ratios of these grains with the isotopic ratios of other elements. The mixing situation leads to a problem with mixing He/C–He/N zone material, similar to that of grain OR1d1m-11 (see Fig. 24 in next section).

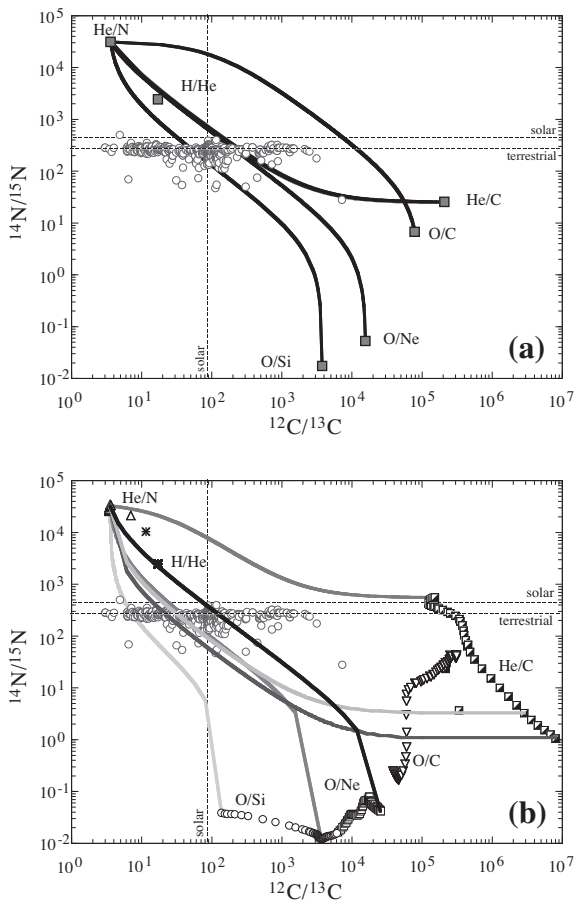

Fig. 17. C and N isotopic compositions of LD graphite grains from Orgueil compared with SN predictions. (a) Mixing lines between the average isotopic compositions of the He/C, O/C, O/Ne, O/Si zones with that of the He/N zone of the Rauscher et al. (2002) 15 $M_{\odot}$ SN model. The shape of the mixing lines is influenced by the relative abundances of C and N in the respective zones in addition to the isotopic ratios. (b) Mixing lines between individual layers within zones (as opposed to averages, as seen in Fig. 17a) of the Rauscher et al. (2002) 15 $M_{\odot}$ SN model. Mixing individual layers provides a better fit to grain data.

4.1.2. Other LD graphites from SNe and limitations of various SN models and mixing calculations

To account for the large ^{12}C, ^{15}N, and ^{18}O excesses, and high ^{26}Al/^{27}Al ratios of a large number of LD grains we need contributions from at least the He/N zone (low ^{12}C/^{13}C and high ^{26}Al/^{27}Al ratios) and from the He/C zone (high ^{12}C/^{13}C ratios, low ^{14}N/^{15}N and ^{16}O/^{18}O ratios). The isotopic compositions of the He/N zone are the result of H burning. Hydrogen burning in the CNO cycle produces low ^{12}C/^{13}C and high ^{14}N/^{15}N ratios and the ^{25}Mg(p,γ)^{26}Al reaction produces ^{26}Al. Partial He burning in the He/C zone results in very high ^{12}C/^{13}C ratios and ^{15}N is synthesized at the bottom of the He/C zone during explosive nucleosynthesis by neutrino reactions on O. Meyer and Bojazi (2011) suggested that heating by the SN shock can also produce ^{15}N by ^{18}F(n,α)^{15}N on ^{18}F produced by ^{14}N(α,γ)^{18}F. The two zones are the only SN zones where C > O (in the inner part of the He/N zone, where H has been completely exhausted).

4.1.2.1. Mixing averages of entire SN zones to explain C and N isotopic ratios. Fig. 17a shows the C and N isotopic ratios of LD graphite grains and the averages of six SN zones of the 15 $M_{\odot}$ model by Rauscher et al. (2002), as well as mixing lines between the He/N zone and the four zones with ^{15}N excesses, i.e., with low ^{14}N/^{15}N ratios. The shape of the mixing line is determined not only by the isotopic ratios of the endpoints, but crucially by the relative abundances of C and N in the two zones to be mixed. For example, the O/C zone has a high C abundance but a low N abundance. As a result, addition of material from the O/C zone to that of the He/N zone first changes the C isotopic ratio while the N isotopic ratio is still dominated by that of the He/N zone, where N is very high. The O/Si zone is very low in both C and N and the mixing curve reflects this. Although the ^{14}N/^{15}N ratios in the O/Ne zone is much lower than in the He/C zone, the mixing curves of these zones with the He/N zone are initially almost identical. One serious problem for mixing with the O/Ne and O/Si zones in the hope of achieving low ^{14}N/^{15}N ratios is that, because of the large abundance of O in these zone, any minor addition of material from these zones will result in an O-rich composition of the mixture way before the C and N isotopic ratios are significantly affected. For example, the mixture of the He/N with the O/Si zone reaches O/C = 100 when ^{12}C/^{13}C = 5 and ^{14}N/^{15}N = 7,500. We also mix material from the He/N, He/C, and O/Si zones under the constraint C = O and determine the ^{14}N/^{15}N ratios for different ^{12}C/^{13}C ratios. We obtain a line that deviates from the He/N-He/C mixing line by less than the line width in the plot. We conclude that contributions from the O-rich SN zones have to be severely restricted to maintain C > O.

4.1.2.2. Mixing individual layers within SN zones to explain C and N isotopic ratios. While Travaglio et al. (1999) mixed averages of whole zones, Fedkin et al. (2010) realized that a better match with the grain data can be achieved if individual layers within zones are used. While the C and N isotopic ratios in the He/N zone of the 15 $M_{\odot}$ model are fairly uniform, they vary over large ranges in the He/

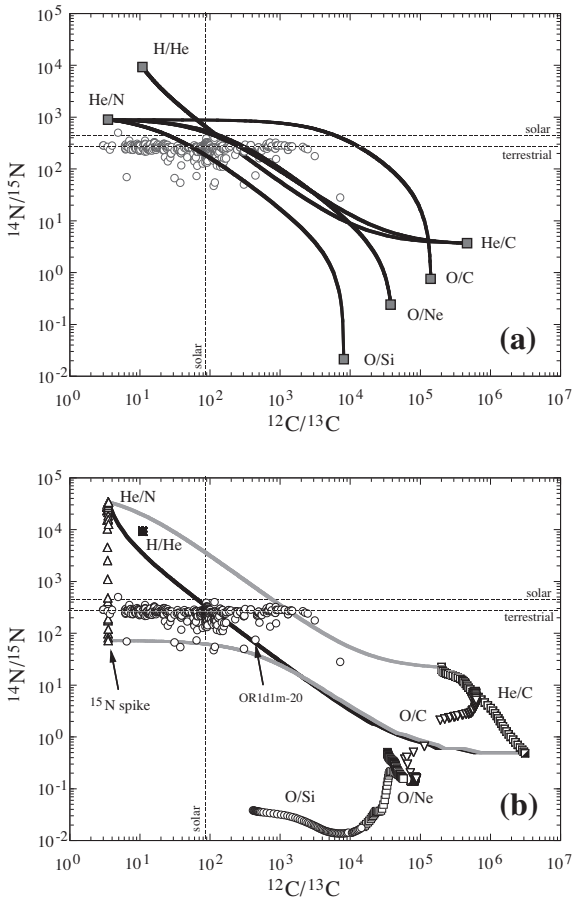

Fig. 18. C and N isotopic compositions of LD graphite grains from Orgueil compared with SN predictions. (a) Mixing lines between the average isotopic compositions of the He/C, O/C, O/Ne, O/Si zones with that of the He/N zone of the Rauscher et al. (2002) 25 $M_{\odot}$ SN model. The shape of the mixing lines is influenced by the relative abundances of C and N in the respective zones. (b) Mixing lines between individual layers within zones (as opposed to averages, as seen in Fig. 18a) of the Rauscher et al. (2002) 25 $M_{\odot}$ SN model. Mixing individual layers of the He/C and He/N zones of this model seems can explain all the grain data.

C zone. Fig. 17b shows C and N isotopic ratio in individual layers of different zones. It also shows mixing lines between a layer from the inner part of the He/N zone (at interior mass 4.0 $M_{\odot}$) and the two layers with extremely different $^{14}N/^{15}N$ ratios in the He/C zone (at 3.1 and 3.788 $M_{\odot}$, respectively) and with the innermost layer (at 1.924 $M_{\odot}$) in the O/Si zone. As can be seen, mixing of the He/N zone with different layers of the He/C zone can cover most of the grain data and maintain C > O but misses a number of grains with very low $^{12}C/^{13}C$ ratios. The mix with the innermost layer of the O/Si zone can cover a fair number of the latter grain compositions but the mixing line intersects the terrestrial $^{14}N/^{15}N$ ratio at an O/C ratio of 2000. It is clear that consideration of individual SN layers within zones increases the complexity of mixing exercises by a large extent, especially if multi-element isotopic compositions, such as this study, are considered.

4.1.2.3. Mixing layers from a 25 $M_{\odot}$ Rauscher SN model to explain C and N isotopic ratios. We also investigated the predictions of the 25 $M_{\odot}$ SN model by Rauscher et al. (2002). Fig. 18a shows C and N isotopic compositions and mixing lines for this model. One peculiar feature of this model is the presence of a ^{15}N spike in the He/N zone in layers where the H abundance goes to zero. This spike results in a lower average $^{14}N/^{15}N$ ratio than in the 15 $M_{\odot}$ SN model. In spite of this fact, the mixing line with the He/C zone still plots above most of the data points, although the $^{14}N/^{15}N$ ratio of the entire He/C zone is also lower than that in the 15 $M_{\odot}$ model. This result appears non-intuitive but is explained by the fact that the N content in the He/C zone is lower than that in the 15 $M_{\odot}$ model. If we plot, as for the 15 $M_{\odot}$ model, the compositions of individual SN layers (Fig. 18b), we see that a mixing line between the layer with the ^{15}N spike and the He/C layer with the lowest $^{14}N/^{15}N$ ratio matches the lowest $^{14}N/^{15}N$ ratios of the grains but falls below all other data points. On the other hand, the mixing line between a layer from the He/N zone outside the spike and the He/C layer with the highest $^{14}N/^{15}N$ ratio falls above all data points. This means that the C and N isotopic compositions of all presolar graphite grains can be explained by mixing between properly selected individual layers from the He/N and He/C zone of the 25 $M_{\odot}$ SN model and, in principle, we do not need any other SN models. This does not mean that graphite grains come only from supernovae of 25 $M_{\odot}$ mass. As we can see from Fig. 18b, mixing in the case where we have a range of C and N isotopic ratios in the He/N and He/C zones does not give a unique solution for a given grain. For example, grain OR1d1m-20 plots close to the mixing line between a He/N layer away from the ^{15}N spike and the layer with the smallest $^{14}N/^{15}N$ ratio in the He/C zone. The $^{16}O/^{18}O$ ratio of the mix that matches the C and N isotopic ratios of this grain is 5. However, the measured $^{16}O/^{18}O$ ratio of this grain is 170. We could try different mixtures of the 25 $M_{\odot}$ Rauscher SN model that reproduce the C and N ratios and see whether a better match to the observed O isotopic ratio can be obtained. We also can try other SN models (e.g., grain OR1d1m-20 plots within the area covered by He/N-He/C mixtures of the 15 $M_{\odot}$ SN model; Fig. 17b). These exercises can get extremely complex and would vastly exceed the scope of this paper.

4.1.2.4. Comparison of Rauscher SN models with other nucleosynthesis models in the literature. In the 20 $M_{\odot}$ SN model by Rauscher et al. (2002), ^{15}N is very low in the He/C zone and the $^{14}N/^{15}N$ ratio is much higher than in the 15 and 25 $M_{\odot}$ SN models, ranging from 14 to 855. This is a special model in which the star experienced some convection before explosion. It has no O/Ne zone. In the 19 $M_{\odot}$ SN model, both ^{14}N and ^{15}N are an order of magnitude higher in the 20 $M_{\odot}$ SN model, but the $^{14}N/^{15}N$ ratio is still high (21–474). In the 21 $M_{\odot}$ SN model, N isotopic abundances in the He/C zone are similar to the abundances in the 25 $M_{\odot}$ SN model. This last model exhibits a tiny ^{15}N spike in the He/N zone but the $^{14}N/^{15}N$ ratio is still 2000, compared to 70 in the 25 $M_{\odot}$ SN model (Fig. 18b).

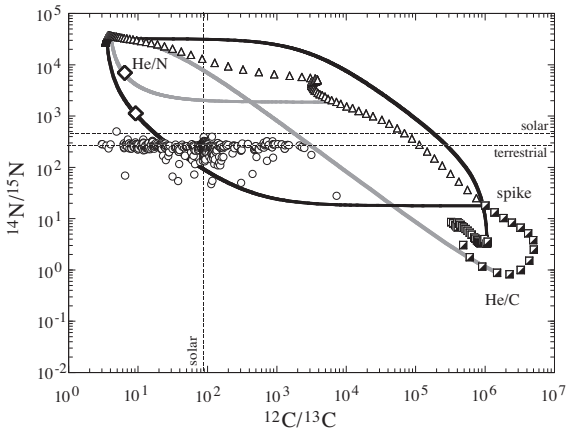

Fig. 19. C and N isotopic compositions of LD graphite grains from Orgueil compared with SN predictions. The figure shows mixing lines between different layers within the He/N zone and the He/C zone of the Heger 12 $M_\odot$ SN model. The mixing lines between the outer region of the He/N zone with layers from the He/C zone completely miss the grain data. Mixing between a layer from the outer He/N zone and an inner layer from this zone and the layer with the ^{15}N spike between the He/N and He/C zone shows that many of the grain data can be covered but only under O > C conditions. The open diamonds indicate the isotopic ratios where the mixture becomes O-rich. Shapes of the mixing lines are influenced by the relative abundances of C and N in the respective zones.

Alexander Heger has computed SN models[3] at all integer solar masses from 12 to 33 $M_\odot$ and at 35 and 40 $M_\odot$. The 12 and 13 $M_\odot$ models have ^{15}N spikes with very low $^{14}N/^{15}N$ ratios (18 and 28, respectively). The spike in these models occurs at the boundary between the He/C and He/N zones. At this layer, ^{18}O is very high but ^{13}C is low. Fig. 19 shows N and C isotopic ratios in the He/N and He/C zones of the 12 $M_\odot$ Heger model. A mixing line between a layer from the outer region of the He/N zone and the layer with the spike misses many LD grains. In addition, since ^{18}O in the layer with the spike is so high, the mixture becomes O-rich at the composition marked by the open diamond. Although $^{14}N/^{15}N$ ratios in the He/C zone are lower, N contents are low and C contents are high, and as a result mixing lines between layers from the outer He/N zone and layers from the He-C zone miss all the LD data. The 15 $M_\odot$ Heger model does not have any ^{15}N spike. Spikes appear again at the 20 $M_\odot$ model and are strongest in the 24 and 25 $M_\odot$ models (with $^{14}N/^{15}N$ ratios of 200, somewhat larger than the ratio of 70 in the 25 $M_\odot$ Rauscher model). Models with higher masses have also spikes but with less intensity. We also looked at the 15, 20, and 25 $M_\odot$ models by Limongi and Chieffi (2003, 2006). The 15 and 20 $M_\odot$ models have $^{14}N/^{15}N$ ratios somewhat lower than terrestrial $^{14}N/^{15}N$ ratios only in the O/Ne and O/Si zones and, as discussed above, any mixing with these zones leads to high O/C ratios. In the 25 $M_\odot$ model, the He/C zone has a lower than terrestrial $^{14}N/^{15}N$ ratio; however, this ratio is constant in the He/C and He/N zones. This would result in only a single mixing line and not provide the variability required to match the C and N isotopic ratios measured in many grains. Furthermore, the maximum $^{26}Al/^{27}Al$ ratio in the He/N zone is about an order of magnitude smaller than in the Rauscher and Heger models. We conclude that the aforementioned models provide no new solutions to SN mixing problems to explain grain data; and, in some cases, are completely incapable of explaining grain data.

4.1.2.5. Mixing SN layers to explain O isotopic ratios. We turn now to the O isotopic ratios. The only SN zone with $^{16}O/^{18}O$ ratios lower than solar is the He/C zone, where partial He-burning produces ^{18}O via the reaction $^{14}N(\alpha,\gamma)^{18}F(\beta^+,\nu)^{18}O$ on the abundant ^{14}N produced by previous H burning in the CNO cycle. Fig. 20a shows C and O ratios in whole zones and mixing lines between them for the 15 $M_\odot$ Rauscher et al. (2002) SN model. Although the $^{16}O/^{18}O$ ratio in the He/N zone is high, the large ^{18}O abundance in the He/C zone results in a mixing line between these zones that is below all the data points of LD graphite grains. Mixing with O-rich zones, all with very high $^{16}O/^{18}O$ ratios, is necessary to reach any grain compositions. We calculated the line along which C/O = 1 when mixing material from the He/N, He/C, and O/C zones (See Fig. 20a). This line is still below most of the data points. Only the region between this line and the He/N–He/C mixing line has C > O, whereas the region above has C < O. The C = O line is even lower for mixing with the O/Ne or O/Si zones, which have higher O/C ratios than the He/C zone. In order to explore whether mixing between specific layers would improve the situation, we mixed a layer in the inner part on the He/N zone (at 4.0 $M_\odot$) with layers in the He/C and O/C zones close to the boundary between these zones (at 3.1 and 2.95 $M_\odot$). The reason for selecting this layer from the O/C zone is that the O/C ratio in this layer is smaller than the more interior layers. The C = O line of such a mixture plots a little higher (Fig. 20a) but most grains still lie above this line. Since the $^{16}O/^{18}O$ ratios in the He/N and He/C zones are quite uniform, we do not gain much more information by considering individual layers. The results from the 25 $M_\odot$ SN model, although somewhat different in detail, are essentially the same. The C = O line calculated for a mixture of material from the He/N, He/C, and O/C zones for this 25 $M_\odot$ SN model is almost identical to that obtained from the 15 $M_\odot$ SN model. The situation is quite different for the 12 $M_\odot$ model by Heger (Fig. 20b). In contrast to the 15 and 25 $M_\odot$ SN models, in the He/N zone the C and O isotopic ratios vary over large ranges. Around the ^{15}N and ^{18}O spike the composition is O-rich (O > C) because of the high ^{18}O abundance. As a consequence, a mixture between layers from the outer He/N zone and the layer with the spike becomes O-rich at a $^{12}C/^{13}C$ ratio of ~10 (indicated by an open diamond in Fig. 20b). However, as one moves into the He/C zone, the C abundance increases rapidly while the $^{18}O/^{16}O$ ratios remains quite low, so that a mixture with such a layer is C-rich throughout and still has $^{18}O/^{16}O$ ratios smaller than those of the grains. On the other hand, mixing with more interior layers (which

[3] Data obtained from: http://webusers.physics.umn.edu/~alex/sollo03/.

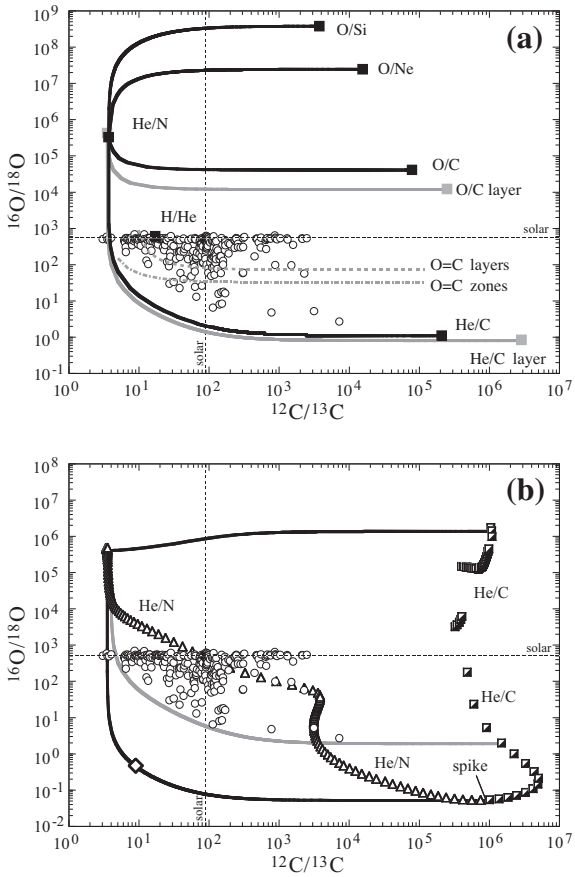

Fig. 20. C and O isotopic compositions of LD graphite grains from Orgueil compared with SN predictions. a) This figure plots mixing lines between averages of the He/N zone and the He/C, O/C, O/Ne, and O/Si zones of the Rauscher et al. (2002) 15 $M_{\odot}$ SN model (black lines). The gray lines indicate mixing lines between specific layers (see text) within the He/N, O/C, and He/C zones. The dot-dash gray O = C line indicates the region where O = C for mixtures between the He/N, He/C, and O/C zones, while the broken gray line is the O = C line for mixing lines between the specific layers from these three zones. (b) Mixing lines between specific layers of the Heger 12 $M_{\odot}$ SN model. Mixing an outer He/N layer with the ^{15}N- and ^{18}O-spike layer does not satisfy grain data and are also O-rich for almost all C isotopic ratios (open diamond indicates O = C). However, a mixture between the outer He/N zone and properly selected layers within the He/C zone can explain all the grain data under C-rich conditions.

have higher $^{18}O/^{16}O$ ratios) results in compositions with higher $^{18}O/^{16}O$ ratios than those of the grains. Thus, mixing between properly selected layers from the He/N and He/C zones can cover all grain data while maintaining C > O conditions.

4.1.2.6. Grain condensation under C-rich vs O-rich conditions. We are now faced with the situation that proper mixing between layers in the 25 $M_{\odot}$ Rauscher model can explain the N and C isotopic compositions of LD grains under C > O conditions, while coverage of the O and C isotopic ratios can be achieved only under C < O conditions. On the other hand, the 12 $M_{\odot}$ Heger model can explain the O and C isotopic ratios of the grains under C-rich conditions but fails to do so for the N and C isotopic ratios. Two possibilities arise as an explanation to the issue of maintaining the C > O condition during graphite grain condensation: either graphite grains can condense from a gas with C < O or, a much more likely scenario, equilibration or contamination is responsible for the shift to normal N and O isotopic ratios in many grains. As for condensation under C < O conditions, we want to point out that condensation from such a mixture is fundamentally different from the proposal by Clayton et al. (1999), Clayton (2011), and Deneault et al. (2003, 2006) that graphite and SiC can condense under O-rich conditions. These authors want to avoid any mixing and thus have the grains condense in the O/Si zone. Since the C, N, O, and Al isotopic ratios in this zone are completely different from those observed in the grains, Clayton (2011) proposes that on their way through the outer zones the grains received their ^{13}C, ^{14}N, ^{18}O, and ^{26}Al in collisions with tiny graphite grains that had condensed in the He-rich zone (Clayton, 2011). However, there is no evidence that ^{13}C, ^{18}O, and ^{26}Al reside mostly in the outer layers of grains while their interior has essentially pure ^{12}C and ^{16}O (Groopman et al., 2012; Zinner and Jadhav, 2012). In some cases, the opposite is observed: the interior of grains have lower $^{16}O/^{18}O$ ratios than the exterior (Stadermann et al., 2005; Groopman et al., 2012). These observations make the Clayton model untenable. We will not pursue the possibility of grain condensation from O-rich gas because we believe that equilibration/contamination is more likely. It is remarkable that so many graphite grains, especially HD grains, have N and O isotopic ratios that are close-to-terrestrial values (Figs. 3 and 4). It has been argued that HD grains have an origin in AGB stars. Such stars are expected to have high $^{14}N/^{15}N$ ratios, and mainstream SiC grains that originate from a similar source, indeed have such high ratios. Grains from AGB stars are also expected to have higher-than-solar $^{16}O/^{18}O$ ratios and most oxide and silicate grains show this signature. Terrestrial values of N and O are produced neither by SNe nor AGB stars; these values are the result of mixing from many stellar sources. The terrestrial ratios found in HD graphites (and some LD graphites) are indicators of the history of the grains in the interstellar medium and/or the solar system. Equilibration in the solar system could have occurred in the early solar system, on the parent body of the host meteorite, or in the laboratory. High-density grains are affected by this equilibration to a much larger extent than LD grains because HD grains have lower trace element abundances to start with. This difference was observed in Murchison graphites as well. Unfortunately, we still do not know where this contamination/equilibration occurred.

4.1.2.7. Mixing SN layers to explain $^{26}Al/^{27}Al$ ratios. Low-density graphite grains are characterized by high inferred $^{26}Al/^{27}Al$ ratios. Fig. 21 shows grain data, the Al and C isotopic ratios predicted for averages of different SN zones by the 15 $M_{\odot}$ Rauscher SN model and mixing lines between the He/N and other SN zones. One problem is immediately apparent: certain grains have $^{26}Al/^{27}Al$ ratios that are larger than ratios predicted by this or any other SN models. This problem has previously been recognized in connection with SiC grains

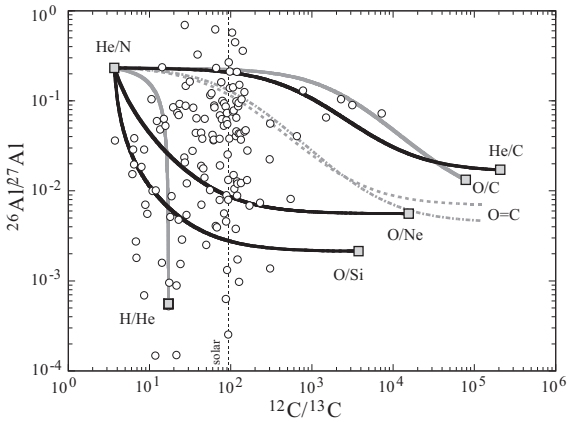

Fig. 21. Derived ^{26}Al/^{27}Al ratios versus ^{12}C/^{13}C ratios of LD graphite grains from Orgueil compared with SN predictions. The figure shows mixing lines between the average isotopic composition of the He/N zone and the averages of H/He, He/C, O/C, O/Ne, and O/Si zones of the Rauscher et al. (2002) 15 $M_{\odot}$ SN model. The grains with highest ^{26}Al/^{27}Al ratios cannot be explained by the mixing of any SN layers or by using other SN models. The broken gray line represents the C = O line for mixing of the He/N, He/C, and O/Ne zones, while the dost-dash gray line is the C = O line for mixing the He/N, He/C, and O/Si zones. Both these scenarios miss most of the grain data.

of type X (e. g., Lin et al., 2010). We believe it is a shortcoming of the SN models and further investigations are required. It is interesting that all the SN models by Woosley and Weaver (1995), Rauscher et al. (2002) and Heger predict very similar maximum ^{26}Al/^{27}Al ratios in the He/N zone. The models by Limongi and Chieffi (2003, 2006) predict lower ratios, but higher ratios are required to match the highest ratios measured in the grains. A second problem is that most LD grains plot below the He/N–He/C mixing line. As for the O isotopic ratios we calculated the C = O lines for mixing of the He/N and He/C zones with the O/Ne and O/Si zones, respectively. As can be seen in Fig. 21, these lines still plot above most of the grain data. Similar to the situation with the O isotopic composition, we are left with three choices: grains can either condense from a gas with C < O, radiogenic ^{26}Mg is lost, or there is a large amount of Al contamination. Our preliminary studies of depth profiles during grain measurements indicate that there is very little loss of radiogenic ^{26}Mg (Zinner and Jadhav, 2012). They also indicate that although some Al contamination is present, it is not clear whether it is large enough to explain the ^{26}Al/^{27}Al ratios of the grains that plot below the C = O lines. We defer more detailed investigations of this problem to a future paper. Mixing curves and C = O lines in the 25 $M_{\odot}$ SN model are similar enough to those in Fig. 21 that the basic conclusions are the same.

We note that most grains with large ^{26}Mg excesses and high inferred ^{26}Al/^{27}Al ratios have significant ^{25}Mg excesses (Fig. 7), which in depth profiles can reach values greater than 3000‰ (unpublished data). This is not necessarily expected because high ^{26}Al/^{27}Al ratios imply substantial contribution from the He/N zone. However, all of the He/N zone and most of the He/C zone are severely depleted in ^{25}Mg and only in the inner layers of the He/C zone do we find ^{25}Mg excesses. In the 15 $M_{\odot}$ Rauscher SN model we have to go very close to the boundary between the O/C and He/C zone to obtain a high enough ^{25}Mg excess for the ^{12}C/^{13}C ratios observed in the grains. This results in a very low ^{14}N/^{15}N ratio (~5). The ^{25}Mg/^{24}Mg ratio in the O/C zone is very high and it might be possible to obtain ^{25}Mg excesses without ending up with too much O. It is interesting that the 25 $M_{\odot}$ Rauscher SN model has a ^{25}Mg spike in the same layers where it has the ^{15}N spike. There the δ^{25}Mg/^{24}Mg value becomes as high as 750‰. Mixing with these layers might help in explaining ^{25}Mg excesses in grains with high ^{26}Al/^{27}Al ratios. Because ^{25}Mg/^{24}Mg ratios vary a lot in the He/N, He/C, and O/C zones, one has to try to select the right layers for mixing.

4.1.2.8. Mixing SN layers to explain Si, Ca, and Ti isotopic ratios. To explain ^{28}Si excesses we need a contribution from the Si/S zone where O burning has resulted in almost pure ^{28}Si and ^{32}S. The He/C zone has modest excesses in ^{29}Si and ^{30}Si, which increase toward the inner part of the zone. However, these excesses are easily overwhelmed if only relatively small amounts of material from the Si/S zone are added. Because ^{28}Si in this zone is so abundant compared to the elements considered so far, there is hardly any effect on the isotopic ratios of these elements. This is not the case for the Ca and Ti isotopes. The abundance of ^{40}Ca is quite high in most of the Si/S zone, ^{48}Ti is highly abundant in the inner part, and ^{42}Ca and ^{46}Ti in the outer portion. In order to explore mixing with the Si/S zone in more detail, for the 25 $M_{\odot}$ Rauscher SN model we obtained a mixture between a layer in the He/N zone (at 8.345 $M_{\odot}$) and a layer from the inner part of the He/C zones (at 7.404 $M_{\odot}$) with fractions of 68.5 and 31.5%, respectively, of these two layers. This mixture has ^{12}C/^{13}C = 100, ^{14}N/^{15}N = 144, ^{16}O/^{18}O = 1.51 and C/O = 8.3. We chose not to go too close to the He/C-O/C boundary, because this would have resulted in a much too high ^{49}Ti excess for this mixture (see Appendix Table A5). We subsequently mixed this component with material from two layers in the inner part (2.242 $M_{\odot}$) and outer part (2.484 $M_{\odot}$) of the Si/S zone. The results for mixtures that resulted in δ^{29}Si/^{28}Si values of –254‰ (or –256‰) and –485‰ are shown for the two cases in Appendix Table A5. To achieve the desired ^{29}Si and ^{30}Si depletions, only up to 2‰ of the Si/S zone has to be added. As expected, the C, N, and Mg isotopic compositions are not affected. The O isotopic ratio and C/O ratio change for the mixture with the outer part because of ^{16}O from the O/Si zone that is still present. Mixture with the outer part increases the δ^{42}Ca/^{40}Ca and δ^{46}Ti/^{48}Ti values, but mixing with the inner part decreases all δ^{i}Ca/^{40}Ca and $\delta^{46,47}$Ti/^{48}Ti values because of the high abundances of ^{40}Ca and ^{48}Ti. The absence of large ^{42}Ca and ^{46}Ti excesses in the grain data (Appendix Table A3) indicate that not much material from the outer Si/S zone has found its way into the grains or that there is substantial fractionation between Ca and Ti on the one and Si on the other hand. Fractionation between Fe and Si has been proposed to explain the lack of ^{54}Fe excesses in SiC X grains (Marhas et al., 2008). However, the presence of ^{44}Ti in SN grains indicates that fractionation between Ti and Si cannot be very strong (Fig. 16). The Si/S zone also contains the short-lived isotopes ^{44}Ti and ^{49}V

($\tau_{1/2} = 337$ days). Although the decay products ^{44}Ca and ^{49}Ti are included in the Si/S material used for the mixing model, without any fractionation between the parent and daughter elements, the effect on δ^{44}Ca/^{40}Ca and δ^{49}Ti/^{48}Ti is small. The Ti/Ca ratio in grains can be high because of the presence of TiC subgrains. We can get high δ^{44}Ca/^{40}Ca values under the assumption of Ti enrichment by factors of 50 and 1000. If we assume an enhancement of the V/Ti ratio by a factor of 10, the contribution of ^{49}V to ^{49}Ti becomes noticeable. But V (which is found in TiC subgrains) and Ti are not observed to be fractionated relative to one another. The lack of ^{49}Ti excesses higher than what can be explained by contributions from the He/C zone confirms the conclusion by Lin et al. (2010) that contribution to ^{49}Ti from ^{49}V decay must be small. Since the abundances of Ca and Ti change substantially within the He/C and Si/S zones we are faced again with the extremely complex problem of selecting appropriate layers and/or appropriate models. Even then it is unlikely that we could explain all the isotopic ratios of a given grain without having to invoke equilibration, contamination, elemental fractionation, and the limitations/failures of the various SN models. Mixing between He/N, He/C, and Si/S zones can, in principle, explain deficits in ^{42,43}Ca and ^{46,47}Ti, the last three of which are observed in some grains (Appendix Table A3). We can also explain ^{44}Ca and ^{46,49,50}Ti excesses (e.g., Figs. 15 and 22). In order to obtain ^{43}Ca excesses, which are seen in some grains, we could choose to mix a layer from the He/C zone that is closer to the He/C–O/C boundary or add some material from the O/C zone. However, that would result in much larger ^{49}Ti and ^{50}Ti excesses than are observed. Titanium-47 excesses, however, cannot be explained by n-capture reactions. Contributions from the decay of ^{47}Ca and ^{47}Sc give rise to an excess of only a few permil (Travaglio et al., 1999). This Ti isotope, with the largest neutron capture cross-section (Bao et al., 2000) among the Ti isotopes, is under-produced by a factor of 5 in the galactic chemical evolution models of Timmes et al. (1995) and its nucleosynthetic origin is not well understood. The occurrence of higher-than-solar ^{47}Ti/^{48}Ti in any SN layer is accompanied by ^{46}Ti/^{48}Ti, ^{49}Ti/^{48}Ti, or ^{50}Ti/^{48}Ti ratios that are higher, as seen in Fig. 22. Furthermore, the regions with ^{47}Ti/^{48}Ti > solar are either in O-rich zones or in the outer Si/S zone, where the ^{47}Ti abundance is so low, that it does not make much of a contribution.

LD grains with inexplicable Ti isotopic patterns are OR1d3m-7, OR1d4m-13, and OR1d3m-23 (Fig. 22; Appendix Table A3); they all have considerable excesses in ^{47}Ti. Apart from a ^{47}Ti excess, grain OR1d4m-13 has a high ^{26}Al/^{27}Al ratio (0.14 ± 0.01, as well as ^{18}O (^{16}O/^{18}O $= 149 \pm 2$) and ^{15}N (^{14}N/^{15}N $= 161 \pm 2$) excesses – all SN signatures. All other isotopic ratios are solar within errors. Grain OR1d3m-7 has a low ^{12}C/^{13}C ratio of ~11 but all the other isotopic ratios are normal or close-to-normal. All except the Ti isotopic ratios of grain OR1d3m-23 are close-to-solar (within errors). Titanium-47 excesses larger than ^{46}Ti excesses have previously been observed in one graphite grain (KE3d-9) from Murchison (Amari and Zinner, 1997), and a SiC grain (M11-151-4), also from Murchison (Nittler and Hoppe, 2005). Interestingly, the SiC grain has a very low ^{12}C/^{13}C ratio of 4.02 ± 0.07 and ^{14}N/^{15}N ratio of 11.6 ± 0.1 (Nittler and Hoppe, 2005). It was originally classified as a nova grain, but its Ti isotopic anomalies indicate a SN origin.

Fig. 23 show the Ca patterns for HD grains, OR1f2m-18 and OR1f2m-o68, and the Ti isotopic pattern for grain OR1f2m-18. These HD grains have much larger Ca and Ti anomalies compared to the LD grains in Fig. 22. Grain OR1f2m-18 has a large ^{47}Ti excess (δ^{47}Ti $= 2120 \pm 354$‰), much greater than the ^{46}Ti excess, which makes its Ti isotopic pattern inexplicable as discussed above. This grain also has a high, inferred ^{41}Ca/^{40}Ca ratio of 0.015 ± 0.003 that can be obtained in the He/C, C/O, and O-rich zones of a Type II SN. The Ca isotopic patterns of grains OR1f2m-18 and OR1f2m-o68 and the ^{46,49}Ti excesses of OR1f2m-18 can be obtained by an admixture of the O-rich to the He/C zones of a Type II SN, as is demonstrated in Fig. 23a and b. Grain OR1f2m-o68 also has large ^{29,30}Si

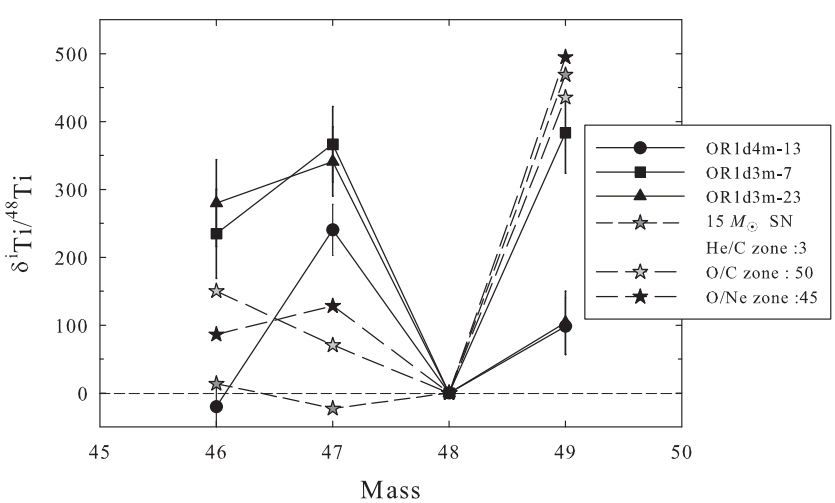

Fig. 22. Ti isotopic patterns of HD graphite grains with a ^{47}Ti anomaly. Titanium-49 excess can be explained by admixture of material from O-rich zones or the He/C zone of the 15 $M_\odot$ SN model (Rauscher et al., 2002). The anomalies in the zones are reduced by appropriate factors as indicated.

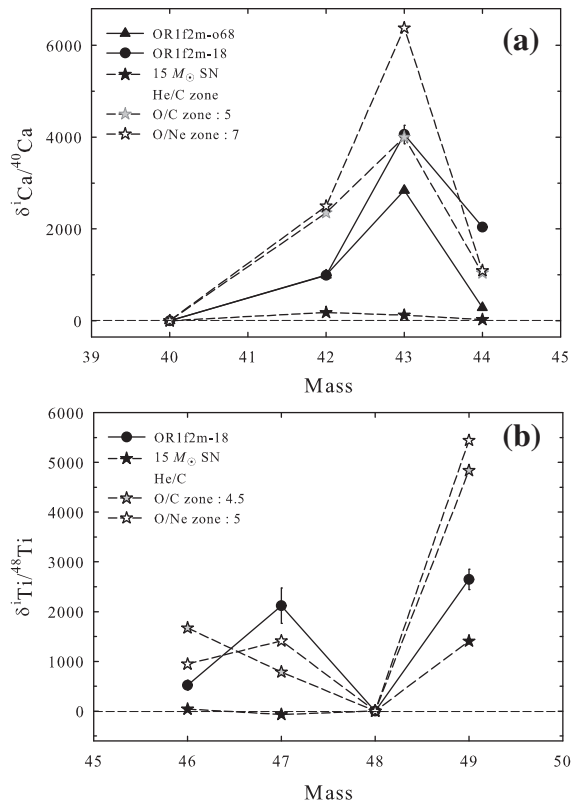

Fig. 23. (a) ^{46,49}Ca and (b) Ti isotopic patterns of HD grains can be reproduced by mixing material from the O-rich zones (O/C and O/Ne) to C-rich zones (Rauscher et al., 2002). The anomalies in the zones are reduced by appropriate factors as indicated.

excesses (δ^{29}Si = 1340 ± 35‰; δ^{30}Si = 896 ± 33‰) and a high inferred ^{41}Ca/^{40}Ca ratio of ~0.014. SiC grains of type C with large ^{29,30}Si excesses have purported SN origin (Hoppe et al., 2010, 2012). Material from the O/C and O/Ne zones can produce such large Ca and Ti anomalies and ^{29,30}Si excesses, but only a small amount of material from these zones has to be added so that the C/O ratio remains greater than 1.

In summary, we conclude that mixing between average compositions of whole zones cannot explain the isotopic compositions of grains very well. The situation is improved if individual layers from different zones are selected but there are still many problems that remain unsolved. The question is whether external reasons for the selection of particular layers can be found. The 25 $M_\odot$ Rauscher SN model and several SN models by Alexander Heger feature ^{15}N (and ^{25}Mg) spikes in the He/N zone. Supernova mixing does a better job of explaining grain data if this layer is selected. Nitrogen-15 in the spike is produced by H burning when this layer at the edge of the H-rich outer region is heated by the SN shock. Another observation from SN mixing exercises is that material from close to the He/C-O/C boundary is needed (e.g., for ^{15}N, ^{25}Mg). This is at the edge of the He-rich region. We wonder whether preferential contributions from these layers have something to do with the "He-wall" and "H-wall". Is it possible that material from interior zones is more intimately mixed when it hits these walls? The 3-D explosion model by Hammer et al. (2010) shows that material from inner zones can penetrate these walls. We hope that future improvements in multi-dimension explosion models can contribute to this question.

We now further demonstrate the mixing problem for a ^{13}C-enriched graphite grain OR1d1m-11. Fig. 24 shows the result of a mixing calculation between different layers of a 15 $M_\odot$ SN model (Rauscher et al., 2002) carried out to reproduce the measured isotopic ratios in OR1d1m-11. Similar to mixing exercises done by Travaglio et al. (1999), Nittler et al. (2008) etc., we mixed material in different proportions from specific layers within the SN zones to achieve the best match between the measured and theoretical ratios. No mathematical minimization routine was performed because of the large uncertainties associated with the stellar models – a quantitative result would lead to a misleading notion that a unique fit is possible for each grain. The calculation was constrained to fit the ^{12}C/^{13}C ratio measured in the grain exactly and the C/O ratio was not allowed be less than 1.

Grain OR1d1m-11 contains large ^{15}N and ^{18}O excesses (^{14}N/^{15}N = 69 ± 1; ^{16}O/^{18}O = 227 ± 45). It also has a high ^{26}Al/^{27}Al ratio of 0.038 ± 0.001. These isotopic signatures point to a SN origin, with major contributions from the He/C zone, for this grain except that it has a very low ^{12}C/^{13}C ratio (6.5), an excess in ^{30}Si (δ^{30}Si = 260 ± 29‰) and a depletion in ^{29}Si (δ^{29}Si = −95 ± 20‰). We have constrained the mixing calculations to reproduce the low ^{12}C/^{13}C ratio of the grain (Fig. 24). This constraint requires that most of the material needs to come from the He/N zone (99.57%). This gives a C/O ratio of 1.5. The only way to keep the ratio from falling below 1 was to obtain material from the C-enriched region at the base of the He/N zone (between masses 3.81–4.7 $M_\odot$). However, the dominant contribution from the He/N zone that has a high ^{14}N/^{15}N ratio causes the mixture to be ^{14}N-enriched and the small contribution from the He/C zone (0.4% at 3.17 $M_\odot$) does not make the mix come close to matching the low ^{14}N/^{15}N ratio seen in this grain. The misfit between the measured N isotopic value and the model calculation cannot be explained by equilibration because the N ratios in the grain and the mix are on opposite sides of the terrestrial ratio (Fig. 24). On the other hand, the much lower ^{18}O excess and smaller ^{26}Al/^{27}Al ratio measured in the grain compared to the values obtained from the model mixture can be attributed to isotopic dilution. A similar mixing exercise using majority of the material from the H-envelope instead of the He/N zone makes the predicted ^{14}N/^{15}N ratio much higher and the C/O ratio of the mix <1. A possible alternative stellar source for such a grain is a nova (Starrfield et al., 1985; Wiescher et al., 1986; Woosley, 1986). The ^{14}N/^{15}N ratio of this grain is higher than that predicted for a typical nova explosion but nevertheless the low ^{12}C/^{13}C and ^{16}O/^{18}O ratios, the large ^{30}Si excess, and the high ^{26}Al/^{27}Al ratio are isotopic signatures predicted for novae (José et al., 2004).

A similar problem arises with grain OR1d4m-8. The low ^{12}C/^{13}C ratio (~14) of this grain makes it difficult to fit all the isotopic ratios. The grain shows evidence for extinct ^{44}Ti (^{44}Ti/^{48}Ti = 0.0027 ± 0.0002), has a very high ^{26}Al/^{27}Al ratio (0.24 ± 0.02), and exhibits excesses in ^{18}O

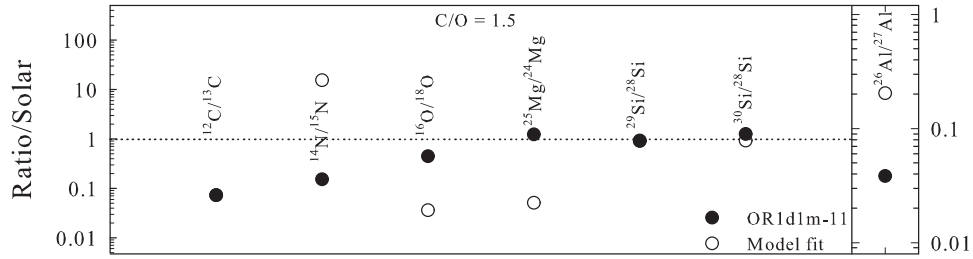

Fig. 24. Comparison between the isotopic ratios measured in grain OR1d1m-11 and those predicted by mixing different layers of the 15 $M_{\odot}$ SN model (Rauscher et al., 2002). The calculation is constrained to produce the low $^{12}C/^{13}C$ ratio (~7) measured in this grain. This mixture has 99.57 % material from the He/N zone, 0.4 % from the He/C zone (at 3.17 $M_{\odot}$), and 0.03 % from the Si/S zone. The resultant C/O ratio of the mixture is 1.5. All the ratios, except $^{26}Al/^{27}Al$, are normalized to solar or terrestrial values, as appropriate.

($^{16}O/^{18}O = 325 \pm 6$), ^{28}Si ($\delta^{29}Si = -232 \pm 9‰$; $\delta^{30}Si = -204 \pm 12‰$) and ^{49}Ti ($\delta^{49}Ti = 203 \pm 10‰$). Since this grain shows evidence for the presence of ^{44}Ti, it has to have originated from a SN. By mixing of the different layers of a SN we are able to reproduce the low $^{12}C/^{13}C$ and $^{16}O/^{18}O$ ratios observed in this grain but at the cost of not being able to fit the Si, Ca, and Ti ratios. Grain OR1d4m-1, with a large ^{28}Si excess and the highest $^{26}Al/^{27}Al$ ratio seen in any graphite grain, also has a sub-solar $^{12}C/^{13}C$ ratio albeit not as low as OR1d4m-8. Nittler et al. (1996) found a graphite grain from Murchison (KE3c-242) with a low $^{12}C/^{13}C$ ratio and a high $^{26}Al/^{27}Al$ ratio, but normal N and O ratios. Another ^{13}C-enriched SiC grain with a large ^{28}Si excess was found by Nittler and Hoppe (2005). Both of these Murchison grains show evidence for extinct ^{44}Ti.

Mixing calculations, like the one presented above for OR1d1m-11, can in principle be done for all putative SN grains like OR1d4m-1 and 4m-8, but they can get extremely cumbersome and complex as more isotopic ratios need to be matched. We currently manually select the best layers that match anomalies observed in grains. In the future, we plan to automate this process.

4.1.2.9. Additional clues from multi-technique correlated studies. One of the goals of this study is to be able to carry out multi-isotopic measurements on the presolar graphites but also save the same grain material for analyses with other techniques. A transmission electron microscope (TEM) study of ultra-microtomed sections of grain OR1d3m-18 by Croat et al. (2011), found this grain to contain TiC subgrains with epitaxial refractory phases, including kamacite, nickel silicide (Ni_2Si), and silicon carbide. A detailed investigation of the microstructure of these TiC subgrains revealed the order of condensation in this graphite: TiC grains condensed first followed by Ni_2Si, Si-rich kamacite (Fe_2Si), SiC, and finally graphite. Graphite grain OR1d3m-18 exhibits all of the phases that equilibrium thermodynamic calculations predict for carbonaceous SN layers (Fedkin et al., 2010). Thus it might not be unreasonable to assume equilibrium scenarios for grain condensation in SN ejecta.

Further, Croat et al. (2012) analyzed an ultra-microtome section of OR1d3m-7 in a TEM. This grain was chosen because of its low $^{12}C/^{13}C$ ratio (~11); it has large $^{46,47,49}Ti$ excesses ($\delta^{46}Ti = 235 \pm 66‰$, $\delta^{47}Ti = 367 \pm 56‰$, $\delta^{49}Ti = 383 \pm 59‰$; Fig. 22; Appendix Table A3). An OsRu-rich metal subgrain was found within the graphite grain, suggesting that stars like Sakurai's object that emit *s*-process element- and ^{13}C-enriched dust (Asplund et al., 1997, 1999), could be sources for graphites with low $^{12}C/^{13}C$ ratios (Croat et al., 2012). Similar refractory subgrains have been found in 2 Murchison HD KFC1 graphites (Croat et al., 2005). As more grains for which we already have isotopic information are analyzed in the TEM, we expect to be able to better constrain the stellar sources of graphites.

4.2. Other stellar sources of Orgueil graphites

Before the advent of the NanoSIMS, HD graphite grains from the Murchison fractions KFB1 and KFC1 have been analyzed for Si isotopes (along with other isotopic systems) with the IMS-3f ion microprobe (e.g., Hoppe et al., 1995). Since HD graphites tend to have a very low abundance of trace elements, the NanoSIMS, with its high sensitivity, allows us to measure the Si isotopes in HD graphites with a much higher precision (Amari et al., 2002, 2005; Jadhav et al., 2006; Meier et al., 2012) than before. These new measurements provide evidence that a large number of HD graphites from Murchison and Orgueil originated in low-metallicity AGB stars (Jadhav et al., 2006; Zinner et al., 2006b). The lack of high-precision measurements of the Si isotopes prior to these NanoSIMS studies could explain why more graphite grains with AGB origins had not been identified before. There is now further evidence from correlated Ne, C, O, Al–Mg isotopic studies (Heck et al., 2009; Meier et al., 2012) that HD grains from the KFB1 and KFC1 Murchison separates originate in low-mass and low-metallicity AGB stars.

In general, the HD grains from the density fractions OR1f, 1g, and 1i, are enriched in ^{29}Si and ^{30}Si. Fig. 6 is a plot of the $\delta^{30}Si/^{28}Si$ values for individual grains from these density fractions as a function of their $^{12}C/^{13}C$ ratios. Most of the HD, ^{30}Si-rich grains contain isotopically light carbon (Jadhav et al., 2006). Such signatures are predicted for low-metallicity AGB stars where more ^{12}C and $^{29,30}Si$ from the He-shell is dredged up into the envelope during the thermally pulsing phase than in stars of solar metallicity (Zinner et al., 2006a). Transmission electron microscope studies of ultra-microtome sections of HD graphites from Murchison (Croat et al., 2005) also assigned an AGB source to the grains based on the high concentration of s-process elements in the

internal carbides. Noble gas (He and Ne) isotopic measurements by Heck et al. (2009) and Meier et al. (2012) also presented evidence for HD graphites from low-metallicity AGB stars. Thus, low-metallicity AGB stars are the most likely source for the HD graphite grains with excesses in ^{30}Si and ^{12}C. Such stars are predicted to also have high C/O ratios and thus, are expected to preferentially condense graphite grains before SiC grains in their ejecta (Lodders and Fegley, 1997; Bernatowicz et al., 2006). This is the most likely reason why no SiC grains with high ^{12}C/^{13}C ratios and large ^{30}Si excesses have been found (Jadhav et al., 2006; Zinner et al., 2006a). Observations by Leisenring et al. (2008) and Sloan et al. (2009) of molecular spectral features of circumstellar dust around AGB stars strengthen this argument. These authors find that the abundance of SiC grains in circumstellar dust shells decreases with decreasing stellar metallicity and is explained by the increasing C/O ratio. Such a scenario favors graphite condensation over SiC. Model calculations of dust formation by Gail et al. (2009) also predict that AGB stars with low-metallicities ($\sim$0.3 $Z_{\odot}$) produce a large fraction of presolar graphite grains.

In Section 3.1 we reported that the N and O isotopic ratios in HD graphites are normal or terrestrial (in case of N) within errors and invoked isotopic equilibrations of these elements in the grains. The original isotopic ratios might have been extremely anomalous. Also, although HD grains seem to be more equilibrated, LD grains might also be partially equilibrated because the anomalies seen in most grains are not as extreme as those expected from SNe (e.g., Figs. 17–23), as discussed in the previous section.

Sixteen graphite grains on the OR1f2m mount have very interesting isotopic anomalies. The C, Ca and Ti isotopic ratios of these grains are listed in Table 2. The nucleosynthetic sources of the 7 grains with ^{12}C/^{13}C ratios less than 20 are discussed in detail by Jadhav et al. (2008). Three of them are SN grains and have been discussed in the previous Section 4.1.1. Here, we will only briefly summarize the results of the other four. We discuss the possible stellar sources of the remaining 9 grains in more detail below.

The four HD grains with low ^{12}C/^{13}C ratios (OR1f2m-9, OR1f2m-29, OR1f2m-34, and OR1f2m-40), which lack evidence for ^{44}Ti, could have condensed in the ejecta of born-again AGB stars, like Sakurai's object (Asplund et al., 1997, 1999). The large Ca and Ti anomalies observed in these grains can be matched by those seen in the undiluted He-shell of a 2 or 3 $M_{\odot}$ AGB star of metallicities, $Z = 0.003$ to 0.02 (Fig. 25a). Hydrogen burning in sources like Sakurai's object can explain the low ^{12}C/^{13}C ratios in such grains (Jadhav et al., 2008). Stellar evolution models (Herwig et al., 1999; Herwig, 2001) indicate that low-mass (2 $M_{\odot}$) stars that have left the AGB may experience a very late-thermal pulse. The He-flash-powered convection zone (rich in freshly produced ^{12}C) extends into the residual H-rich envelope and causes convective H burning via the CN cycle. This converts ^{12}C to ^{13}C and reduces the ^{12}C/^{13}C ratio. Since in the post-AGB phase of stellar evolution, most of the envelope has already been ejected as a planetary nebula, the residual envelope has a limited supply of protons. The H is exhausted before ^{14}N becomes more abundant than ^{12}C and the envelope remains C-rich. Furthermore, because the envelope is small, the Ca and Ti from the intershell are not diluted and these elements maintain their huge isotopic anomalies.

The Ti isotopic patterns for grains OR1f2m-21, OR1f2m-39, and OR1f2m-33 are shown in Fig. 25b. The Ca isotopic ratios are essential normal (Table 2) and hence are not diagnostic in determining the stellar sources of these grains. Grain OR1f2m-39 has a relatively small inferred ^{41}Ca/^{40}Ca ratio (0.0006 ± 0.0004), comparable to that expected from AGB stars, which are in the range of 10^{-5}–10^{-4} (Wasserburg et al., 1995b; Amari et al., 1996; Gallino et al., 1998). All 3 grains have ^{12}C/^{13}C ratios greater than 300, and the Ti isotopic patterns can be matched with that of the O/C and O/Ne zones of a 15 $M_{\odot}$ SN. Obtaining these Ti anomalies using material from O-rich zones leads to a mixture that has C > O making a SN source less viable, especially since these grains do not exhibit any other SN signatures. These Ti isotopic ratios are higher than those expected from envelopes of AGB star but the He-shells of these stars produce extremely large Ti anomalies. Similar Ti isotopic patterns are observed in the He-shell of a 2 and 3 $M_{\odot}$ AGB star of metallicities, $Z = 0.02$ and 0.003, respectively (Fig. 25b). These grains are ^{12}C-enriched unlike the grains in Fig. 25a. Models of post-AGB stars predict that stars suffering a very late-thermal pulse can produce both sub-solar and higher than solar ^{12}C/^{13}C ratios during different stages of their lifecycle (unpublished data from Jadhav et al. NIC-XII, 2012; Herwig et al., 2011).

We found two grains in the HD fraction, OR1g1m-33 and OR1f1m-5, with high ^{14}N/^{15}N ratios of 1437 ± 30 and 571 ± 15, respectively. Both these grains are ^{13}C-enriched with ^{12}C/^{13}C ratios $\sim$14 (Fig. 3b; Section 4.1.2). The grains have solar values (within errors) of ^{16}O/^{18}O, ^{29}Si/^{28}Si, and ^{30}Si/^{28}Si. There is no other isotopic information available for these two grains. While it is difficult to constrain the stellar source on the basis of C and N isotopes alone, we suggest J-type stars as possible sources for these grains. Recently, Hedrosa et al. (2012) measured N isotopic ratios in seven galactic J-type stars with ^{12}C/^{13}C ratios between 2 and 10. They found the ^{14}N/^{15}N ratios in these stars to be both much higher and lower than the terrestrial value. J-type stars have also been proposed to be the source of type AB SiC grains that have ^{12}C/^{13}C ratios < 10, lower and higher than terrestrial ^{14}N/^{15}N ratios, and Si isotopic compositions that plot along the mainstream line for SiC grains (Amari et al., 2001).

Thus, HD graphites from Orgueil seem to have several stellar sources. We have seen evidence for SN grains (Section 4.1), graphites from low-metallicity AGB stars, grains that come from a ^{13}C-enriched stellar source (like Sakurai's object) that supplied an abundance of neutrons that give rise to extremely large Ca and Ti excesses. We also see some preliminary evidence for graphites from J-type stars.

4.3. Comparison with Murchison graphite

Orgueil graphite grains appear to be similar to Murchison graphite grains in their isotopic properties. Morphologically, the onion-type grains observed in Orgueil are similar to the HD Murchison graphites but unlike in Murchison, are abundant in both the LD and HD fractions. Very few

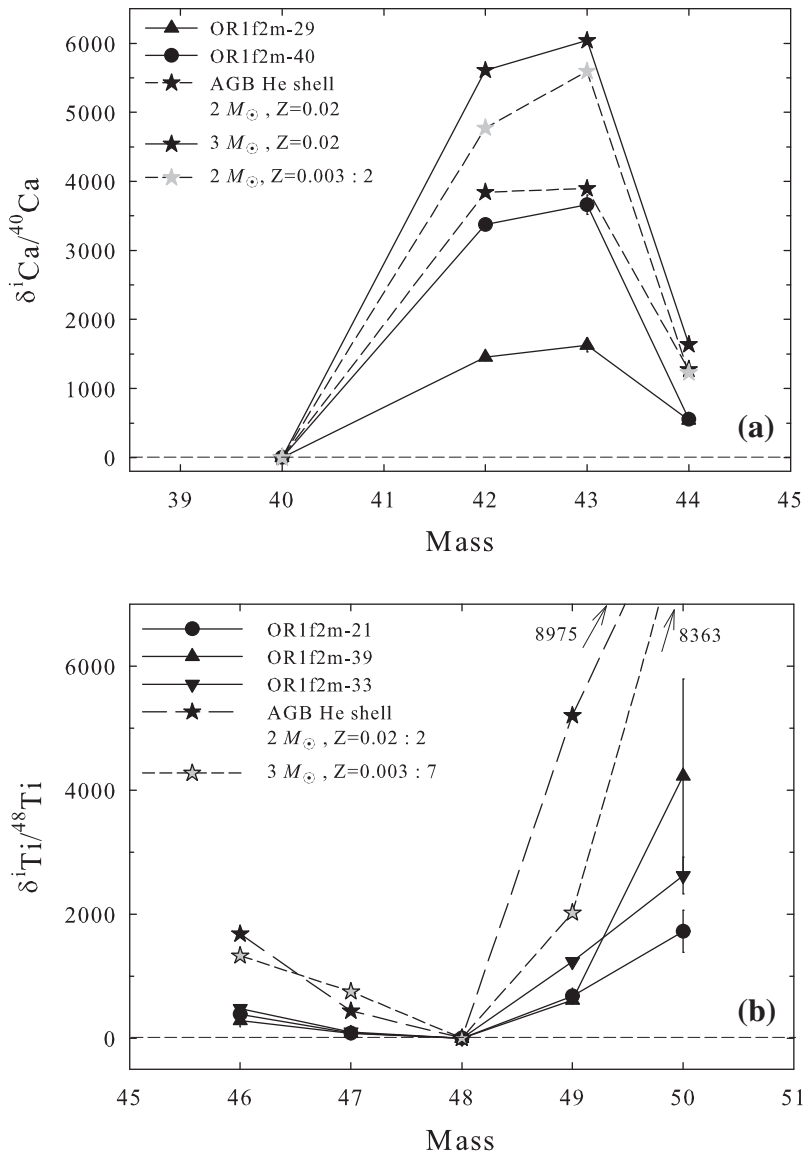

Fig. 25. (a) Ca isotopic patterns for ^{13}C-enriched HD grains OR1f2m-29 and OR1f2m-40, compared to those predicted for the He-shell of 2 $M_\odot$ ($Z = 0.003$ and 0.02) and 3 $M_\odot$ ($Z = 0.02$) AGB stars (Gallino et al., 1998). (b) The Ti isotopic patterns of three ^{12}C-enriched HD grains can be matched by the patterns predicted for the He-shell of 2 $M_\odot$ ($Z = 0.02$) and 3 $M_\odot$ ($Z = 0.003$) AGB stars (Gallino et al., 1998). The predicted anomalies are scaled down by the factors indicated.

cauliflower grains (see Fig. 2 in Hoppe et al., 1995) have been observed in any density fraction of Orgueil. Murchison LD graphites were larger than the HD graphites (Hoppe et al., 1995). We might be seeing an opposite trend in Orgueil size distributions (see Section 3 for grain size discussion). A larger fraction (55%) of Orgueil HD graphites have grain sizes > 4 μm compared to the LD grains (50%). If this small difference is real then we must caution the reader about bias from two sources: 1. Grains are picked out of the macromolecular carbon and hence subject to a selection bias. 2. The nature of the macromolecular carbon (e.g., density and quantity) in the LD and HD fractions might be different and this might lead to difficulty in finding grains in a certain size range.

The lack of a large range of N anomalies is a common trend in the graphites from both meteorites (Hoppe et al., 1995). In the KE3 fraction (1.65–1.72 g cm^{-3}) from Murchison about a third of the grains are from supernovae. The abundance of ^{18}O-rich grains decreases with increasing density and, in fact, such grains have not been observed in the highest Murchison density fraction KFC1 (2.15–2.20 g cm^{-3}). A similar trend is observed in the abundance of ^{18}O enriched grains in the density fractions of Orgueil. NanoSIMS analyses of HD graphite grains (KFB1) from Murchison (Amari et al., 2005) indicate that they also have ^{30}Si excesses, similar to the ones seen in the HD fractions from Orgueil (OR1f, 1g, and 1i), and they are thus believed to have originated from low-metallicity AGB stars. There is no Ca and Ti isotopic evidence for Murchison graphite grains from born-again AGB stars, like the ones discussed by Jadhav et al. (2008). However, a population of grains with ^{12}C/^{13}C around 10 exists in all the density fractions

of Murchison as well. Additional isotopic measurements on these ^{13}C-enriched graphites from Murchison will be needed to better constrain their stellar sources.

Huss and Lewis (1995) claim that a homogenous mixture of presolar grains was inherited by members of all the chondritic classes of meteorites and survived in the most primitive of these classes. After parent body formation, thermal and aqueous alteration processes could have affected the presolar grain populations to varying extents. Thus, the presolar grain populations from Orgueil and Murchison and their abundances are expected to differ from one another. Although both meteorites show very little evidence of thermal metamorphism, the matrix mineralogy of Orgueil indicates extensive aqueous alteration (e.g., McSween, 1979). It is also possible that the initial presolar grain population was sorted in the early solar system according to physical properties or selectively destroyed by partial evaporation of solids. The destruction of certain presolar phases or of a certain type (e.g., cauliflower graphites in Orgueil) within a certain phase, in the laboratory during chemical separation techniques also cannot be ruled out.

4.4. Unresolved issues

(a) Nitrogen, O, and Mg (and sometimes Si) isotopic data on HD grains points to the fact that these isotopic ratios were diluted/equilibrated. This equilibration could have occurred in the laboratory, the parent body, the solar nebula or the interstellar medium. While it is obvious that the HD grains are affected the most by the equilibration due to the low trace elemental abundances, the exact mechanism for such a dilution process needs to be investigated.

(b) Low-density graphite grains from both Murchison and Orgueil are mainly supernova grains while HD grains have multiple sources and originate in low-metallicity and born-again AGB stars, SNe, and possibly J-type stars. Multiple stellar sources for grains of different densities could be an inherent property of presolar graphite grains in Orgueil or an artifact. Every density fraction of Orgueil contains a large amount of the macromolecular carbon that was mentioned in Section 2.2. Most graphite grains are found embedded in this material. It is entirely possible that grains from different densities remain embedded in this carbonaceous material and were not separated completely during the density separation. Since the average density of a fraction is measured, grains with different densities could be mixed in with the others, making the density separates imperfect.

The presence of this macromolecular carbon in all the density fractions of Orgueil graphites also makes it difficult to carry out meaningful abundance calculations of presolar graphite grains from Orgueil, because grains embedded and hidden in this IOM will not be included in the calculations. It is essential to study the structure and composition of this macromolecular carbon to further refine the chemical separation procedure used to extract presolar graphite grains from meteorites, especially those similar to Orgueil that are very rich in organics.

(c) Isotopic studies of subgrains found within graphites similar to the one carried out by Stadermann et al. (2005) are very important to establish the exact nature and source of the isotopic anomalies seen in these grains. For example, most Ti measured in the graphites is found in subgrains while the Ca is uniformly distributed in the host grain. As discussed by Groopman et al. (2012), the parent grain and its subgrains could have formed under completely different condensation conditions and the Ca and Ti anomalies we find in a single grain could originate from distinct layers of the stellar source. Such a scenario is not considered when the stellar sources of the grains are discussed based on the isotopic ratios measured in the whole grain.

(d) In the HD fraction OR1f we found grains with extremely large Ca and Ti anomalies but almost normal N, O, Mg, and Si isotopic ratios. Neutron capture reactions that affect the Ca and Ti isotopes should have also affected the Mg and Si isotopes considerably. The nature of the equilibrating processes that affect only Mg and Si isotopes, and not Ca and Ti isotopes needs to be identified and better understood. Sources of possible contamination also need to be identified as contamination makes the determination of stellar sources of these grains very complicated (e.g., Barzyk et al., 2007).

5. FUTURE PERSPECTIVES

Presolar graphite grains from Orgueil have multiple stellar sources. In this study, we presented isotopic evidence for graphite grains from supernovae, low-metallicity AGB stars, and born-again AGB stars. Sakurai's object-type post-AGB stars are a likely source of grains with low ^{12}C/^{13}C ratios and extreme Ca and Ti anomalies, while J-type stars could be the source of ^{13}C- and ^{14}N-enriched graphites. Further coordinated isotopic studies are required to determine the nature of these sources. Extensive correlated isotopic measurements are planned for a large fraction of the grains that remain intact after the SIMS analyses presented in this paper. Resonant ionization mass spectrometry (RIMS) analyses of Mo, Zr, Sr, and Ba isotopic ratios (e.g., Nicolussi et al., 1997, 1998a,b,c; Savina et al., 2003) are planned and will be essential to completely characterize these grains and constrain their stellar sources. Raman spectroscopy and TEM studies of these grains will help elucidate the chemical environments in which these grains condensed and determine the structural differences between Murchison and Orgueil graphites.

ACKNOWLEDGMENTS

We thank the Associate Editor, J.N. Goswami, and reviewers A.M. Davis, L.R. Nittler, and P. Heck for detailed reviews that have made this a much improved manuscript. This work was supported by NASA Grant NNG05GF81G. We thank Frank Stadermann for Auger Nanoprobe time to obtain SE images of some of the grains in this study. Tim Smolar's assistance with the NanoSIMS is greatly appreciated.

APPENDIX A. SUPPLEMENTARY DATA

Supplementary data associated with this article can be found, in the online version, at http://dx.doi.org/10.1016/j.gca.2013.01.018.

REFERENCES

Amari S. and Zinner E. (1997) Supernova grains from meteorites. In *Astrophysical Implications of the Laboratory Study of Presolar Materials* (eds. T. J. Bernatowicz and E. Zinner). AIP, pp. 287–305.

Amari S., Anders E., Virag A. and Zinner E. (1990) Interstellar graphite in meteorites. *Nature* **345**, 238–240.

Amari S., Hoppe P., Zinner E. and Lewis R. S. (1992) Interstellar SiC with unusual isotopic compositions: Grains from a supernova? *Astrophys. J.* **394**, L43–L46.

Amari S., Lewis R. S. and Anders E. (1994) Interstellar grains in meteorites: I. Isolation of SiC, graphite, and diamond; size distributions of SiC and graphite. *Geochim. Cosmochim. Acta* **58**, 459–470.

Amari S., Lewis R. S. and Anders E. (1995a) Interstellar grains in meteorites: III. Graphite and its noble gases. *Geochim. Cosmochim. Acta* **59**, 1411–1426.

Amari S., Zinner E. and Lewis R. S. (1995b) Large ^{18}O excesses in circumstellar graphite grains from the Murchison meteorite: Indication of a massive star-origin. *Astrophys. J.* **447**, L147–L150.

Amari S., Zinner E. and Lewis R. S. (1996) ^{41}Ca in presolar graphite of supernova origin. *Astrophys. J.* **470**, L101–L104.

Amari S., Nittler L. R., Zinner E., Gallino R., Lugaro M. and Lewis R. S. (2001) Presolar SiC grains of type A and B: Their isotopic compositions and stellar origins. *Astrophys. J.* **559**, 463–483.

Amari S., Nguyen A. and Zinner E. (2002) Multi-element isotopic analysis of presolar graphite fraction KFA1 from the Murchison meteorite. *Meteorit. Planet. Sci.* **37**, A11 (abstr.).

Amari S., Zinner E. and Lewis R. S. (2005) Isotopic analysis of presolar graphite from the KFB1 Murchison separate. *Meteorit. Planet. Sci.* **40**, A15 (abstr.).

Amari S., Zinner E. and Gallino R. (2012) Presolar graphite from the Murchison meteorite; puzzles related to its origins. *Lunar Planet. Sci. XLIII*. #1031 (abstr.).

Asplund M., Gustafsson B., Lambert D. L. and Rao Kameswara N. (1997) A stellar endgame – The born-again Sakurai's object. *Astron. Astrophys.* **321**, L17–L20.

Asplund M., Lambert D. L., Kipper T., Pollacco D. and Shetrone M. D. (1999) The rapid evolution of the born-again giant Sakurai's object. *Astron. Astrophys.* **343**, 507–518.

Barzyk J. G., Savina M. R., Davis A. M., Gallino R., Gyngard F., Amari S., Zinner E., Pellin M. J., Lewis R. S. and Clayton R. N. (2007) Constraining the ^{13}C neutron source in AGB stars through isotopic analysis of trace elements in presolar SiC. *Meteorit. Planet. Sci.* **42**, 1103–1119.

Bernatowicz T. J., Croat T. K. and Daulton T. L. (2006) Origin and evolution of carbonaceous presolar grains in stellar environments. In *Meteorites and the Early Solar System II* (eds. D. S. Lauretta and H. Y. McSween Jr.). Univ. of Arizona, Tucson, pp. 109–126.

Besmehn A. and Hoppe P. (2003) A NanoSIMS study of Si- and Ca–Ti-isotopic compositions of presolar silicon carbide grains from supernovae. *Geochim. Cosmochim. Acta* **67**, 4693–4703.

Bao Z. Y., Beer H., Käppeler F., Voss K., Wisshak K. and Rauscher T. (2000) Neutron cross sections for nucleosynthesis studies. *Atomic Data and Nuclear Data Tables* **76**, 70.

Busso M., Gallino R. and Wasserburg G. J. (1999) Nucleosynthesis in asymptotic giant branch stars: Relevance for Galactic enrichment and solar system formation. *Ann. Rev. Astron. Astrophys.* **37**, 239–309.

Clayton D. D. (2011) A new astronomy with radioactivity: Radiogenic carbon chemistry. *New Astron. Rev.* **55**, 155–165.

Clayton D. D., Liu W. and Dalgarno A. (1999) Condensation of carbon in radioactive supernova gas. *Science* **283**, 1290–1292.

Cristallo S., Piersanti L., Straniero O., Gallino R., Dominguez I., Abia C., Di Rico G., Quintini M. and Bisterzo S. (2011) Evolution, nucleosynthesis, and yields of low-mass asymptotic giant branch stars at different metallicities. II. The FRUITY database. *Astrophys. J. Suppl.* **197**, 21.

Croat T. K., Bernatowicz T., Amari S., Messenger S. and Stadermann F. J. (2003) Structural, chemical, and isotopic microanalytical investigations of graphite from supernovae. *Geochim. Cosmochim. Acta* **67**, 4705–4725.

Croat T. K., Stadermann F. J. and Bernatowicz T. J. (2005) Presolar graphite from AGB stars: Microstructure and *s*-process enrichment. *Astrophys. J.* **631**, 976–987.

Croat T. K., Stadermann F. J. and Bernatowicz T. J. (2010) Unusual ^{29,30}Si-rich SiCs of massive star origin found within graphite from the Murchison meteorite. *Astron. J.* **139**, 2159–2169.

Croat T. K., Jadhav M., Lebsack E. and Bernatowicz T. J. (2011) A unique supernova graphite: Contemporaneous condensation of all things carbonaceous. *Lunar Planet Sci. XLII*. #1533 (abstr.).

Croat T. K., Berg T., Jadhav M. and Bernatowicz T. J. (2012) Presolar refractory metal nuggets. *Lunar Planet. Sci. XLIII*. #1503 (abstr.).

Davis A. M., Gallino R., Straniero O., Dominguez I. and Lugaro M. (2003) Heavy element nucleosynthesis in low metallicity, low mass AGB stars. *Lunar Planet. Sci. XXXIV*. #2043 (abstr.).

Deneault E. A.-N., Clayton D. D. and Heger A. (2003) Supernova reverse shocks: SiC growth and isotopic composition. *Astrophys. J.* **594**, 312–325.

Deneault E. A.-N., Clayton D. D. and Meyer B. S. (2006) Growth of carbon grains in supernova ejecta. *Astrophys. J.* **638**, 234–240.

Ebisuzaki T. and Shibazaki N. (1988) The effects of mixing of the ejecta on the hard X-ray emissions from SN 1987A. *Astrophys. J.* **327**, L5–L8.

Fedkin A. V., Meyer B. S. and Grossman L. (2010) Condensation and mixing in supernova ejecta. *Geochim. Cosmochim. Acta* **74**, 3642–3658.

Flesch G. D., Capellan J. and Svec H. J. (1966) The abundance of the vanadium isotopes from sources of geochemical interest. *Adv. Mass Spec.* **III**, 571–574.

Gail H.-P., Zhukovska S. V., Hoppe P. and Trieloff M. (2009) Stardust from asymptotic giant branch stars. *Astrophys. J.* **698**, 1136–1154.

Gallino R., Arlandini C., Busso M., Lugaro M., Travaglio C., Straniero O., Chieffi A. and Limongi M. (1998) Evolution and nucleosynthesis in low-mass asymptotic giant branch stars. II. Neutron capture and the s-process. *Astrophys. J.* **497**, 388–403.

Groopman E., Bernatowicz T. and Zinner E. (2012) C, N, and O isotopic heterogeneities in low-density supernova graphite grains from Orgueil. *Astrophys. J. Lett.* **754**, L8.

Gyngard F., Nittler L. R. and Zinner E. (2010) Presolar SiC grains of Type C. *Meteorit. Planet. Sci.* **45**, A72.

Hammer N. J., Janka H.-T. and Müller E. (2010) Three-dimensional simulations of mixing instabilities in supernova explosions. *Astrophys. J.* **714**, 1371–1385.

Heck P. R., Amari S., Hoppe P., Baur H., Lewis R. S. and Wieler R. (2009) Ne isotopes in individual presolar graphite grains from the Murchison meteorite together with He, C, O, Mg–Al isotopic analyses as tracers of their origins. *Astrophys. J.* **701**, 1415–1425.

Hedrosa R. P., Abia C., Plez B. and Domínguez I. (2012) Nitrogen isotopic ratios in galactic AGB carbon stars. In *Proceedings of the International Symposium "Nuclei in the Cosmos – XII"*,

August 5–12, 2012. Cairns, Australia. Proceedings of Science, PoS (NIC-XII) 006.

Herant M., Benz W., Hix W. R., Fryer C. L. and Colgate S. A. (1994) Inside the supernova: A powerful convective engine. *Astrophys. J.* **435**, 339–361.

Herwig F. (2001) Internal mixing and surface abundance of [WC]-CSPN. *Astrophys. Space Sci.* **275**, 15–26.

Herwig F., Blöcker T., Langer N. and Driebe T. (1999) On the formation of hydrogen-deficient post-AGB stars. *Astron. Astrophys.* **349**, L5–L8.

Herwig F., Pignatari M., Woodward P. R., Porter D. H., Rockefeller G., Fryer C. L., Bennett M. and Hirschi R. (2011) Convective-reactive proton-^{12}C combustion in Sakurai's object (V4334 Sagittarii) and implication for the evolution and yields from the first generation of stars. *Astrophys. J.* **727**, 89.

Hoppe P., Amari S., Zinner E., Ireland T. and Lewis R. S. (1994) Carbon, nitrogen, magnesium, silicon and titanium isotopic compositions of single interstellar silicon carbide grains from the Murchison carbonaceous chondrite. *Astrophys. J.* **430**, 870–890.

Hoppe P., Amari S., Zinner E. and Lewis R. S. (1995) Isotopic compositions of C, N, O, Mg, and Si, trace element abundances, and morphologies of single circumstellar graphite grains in four density fractions from the Murchison meteorite. *Geochim. Cosmochim. Acta* **59**, 4029–4056.

Hoppe P., Strebel R., Eberhardt P., Amari S. and Lewis R. S. (1996) Type II supernova matter in a silicon carbide grain from the Murchison meteorite. *Science* **272**, 1314–1316.

Hoppe P., Annen P., Strebel R., Eberhardt P., Amari S. and Lewis R. S. (1997) Circumstellar SiC grains of Type Z: Evidence for extensive He shell dredge-up in low-metallicity low-mass AGB stars. *Lunar Planet. Sci.* **XXVIII**, 599–600 (abstr.).

Hoppe P., Strebel R., Eberhardt P., Amari S. and Lewis R. S. (2000) Isotopic properties of silicon carbide X grains from the Murchison meteorite in the size range 0.5–1.5 μm. *Meteorit. Planet. Sci.* **35**, 1157–1176.

Hoppe P., Leitner J., Gröner E., Marhas K. K., Meyer B. S. and Amari S. (2010) NanoSIMS studies of small presolar SiC grains: New insights into supernova nucleosynthesis, chemistry, and dust formation. *Astrophys. J.* **719**, 1370–1384.

Hoppe P., Fujiya W. and Zinner E. (2012) Sulfur molecule chemistry in supernova ejecta recorded by silicon carbide stardust. *Astrophys. J. Lett.* **745**, L26–L30.

Hughes J. P., Rakowski C. E., Burrows D. N. and Slane P. O. (2000) Nucleosynthesis and mixing in Cassiopeia A. *Astrophys. J.* **528**, L109–L113.

Huss G. R. and Lewis R. S. (1995) Presolar diamond, SiC, and graphite in primitive chondrites: Abundances as a function of meteorite class and petrologic type. *Geochim. Cosmochim. Acta* **59**, 115–160.

Jadhav M., Amari S., Zinner E. and Maruoka T. (2006) Isotopic analysis of presolar graphite grains from Orgueil. *New Astron. Rev.* **50**, 591–595.

Jadhav M., Amari S., Marhas K. K., Zinner E., Maruoka T. and Gallino R. (2008) New stellar sources for high-density, presolar graphite grains. *Astrophys. J.* **682**, 1479–1485.

José J., Hernanz M., Amari S., Lodders K. and Zinner E. (2004) The imprint of nova nucleosynthesis in presolar grains. *Astrophys. J.* **612**, 414–428.

Joggerst C. C., Woosley S. E. and Heger A. (2009) Mixing in zero- and solar-metallicity supernovae. *Astrophys. J.* **693**, 1780–1802.

Junk G. and Svec H. J. (1958) The absolute abundance of the nitrogen isotopes in the atmosphere and compressed gas from various sources. *Geochim. Cosmochim. Acta* **14**, 234–243.

Kifonidis K., Plewa T., Janka H.-T. and Müller E. (2003) Non-spherical core collapse supernovae I. Neutrino-driven convection, Rayleigh-Taylor instabilities, and the formation and propagation of metal clumps. *Astron. Astrophys.* **408**, 621–649.

Lambert D. L., Gustafsson B., Eriksson K. and Hinkle K. H. (1986) The chemical composition of carbon stars. I. Carbon, nitrogen, and oxygen in 30 cool carbon stars in the galactic disk. *Astrophys. J. Suppl.* **62**, 373–425.

Larimer J. W. (1975) The effect of C/O ratio on the condensation of planetary material. *Geochim. Cosmochim. Acta* **39**, 389–392.

Leisenring J. M., Kemper F. and Sloan G. C. (2008) Effects of metallicity on the chemical composition of carbon stars. *Astrophys. J.* **681**, 1557–1573.

Lewis R. S., Anders E. and Draine B. T. (1989) Properties, detectability and origin of interstellar diamonds in meteorites. *Nature* **339**, 117–121.

Limongi M. and Chieffi A. (2003) Evolution, explosion, and nucleosynthesis of core-collapse supernovae. *Astrophys. J.* **592**, 404–433.

Limongi M. and Chieffi A. (2006) The nucleosynthesis of ^{26}Al and ^{60}Fe in solar metallicity stars extending in mass from 11 to 120 M: The hydrostatic and explosive contributions. *Astrophys. J.* **647**, 483–500.

Lin Y., Gyngard F. and Zinner E. (2010) Isotopic analysis of supernova SiC and Si_3N_4 grains from the Qingzhen (EH3) chondrite. *Astrophys. J.* **709**, 1157–1173.

Lodders K. (2003) Solar system abundances and condensation temperatures of the elements. *Astrophys. J.* **591**, 1220–1247.

Lodders K. and Fegley, Jr., B. (1995) The origin of circumstellar silicon carbide grains found in meteorites. *Meteoritics* **30**, 661–678.

Lodders K. and Fegley, Jr., B. (1997) Condensation chemistry of carbon stars. In *Astrophysical Implications of the Laboratory Study of Presolar Materials* (eds. T. J. Bernatowicz and E. Zinner). AIP, pp. 391–423.

Marhas K. K., Amari S., Gyngard F., Zinner E. and Gallino R. (2008) Iron and nickel isotopic ratios in presolar SiC grains. *Astrophys. J.* **689**, 622–645.

Marty B., Chaussidon M., Wiens R. C., Jurewicz A. J. G. and Burnett D. S. (2011) A ^{15}N-poor isotopic composition for the solar system as shown by Genesis solar wind samples. *Science* **332**, 1533–1536.

McKeegan K. D., Kallio A. P. A., Heber V. S., Jarzebinski G., Mao P. H., Coath C. D., Kunihiro T., Wiens R. C., Nordholt J. E., Moses, Jr., R. W., Reisenfeld D. B., Jurewicz A. J. G. and Burnett D. S. (2011) The oxygen isotopic composition of the Sun inferred from captured solar wind. *Science* **332**, 1528–1532.

McSween, Jr., H. Y. (1979) Are carbonaceous chondrites primitive or processed? *Rev. Geophys. Space Phys.* **17**, 1059–1078.

Meier M. M. M., Heck P. R., Amari S., Baur H. and Wieler R. (2012) Graphite grains in supernova ejecta – Insights from a noble gas study of 91 individual KFC1 presolar graphite grains from the Murchison meteorite. *Geochim. Cosmochim. Acta* **76**, 147–160.

Meyer B. S. and Bojazi M. J. (2011) Production of nitrogen-15 in explosive helium burning and supernova presolar grains. *Lunar Planet. Sci. XLII*. #2376 (abstr.).

Meyer B. S. and Zinner E. (2006) Nucleosynthesis. In *Meteorites and the Early Solar System II* (eds. D. S. Lauretta and H. Y. McSween Jr.). Univ. of Arizona, Tucson, pp. 69–108.

Meyer B. S., Weaver T. A. and Woosley S. E. (1995) Isotope source table for a 25 $M_\odot$ supernova. *Meteoritics* **30**, 325–334.

Müller E., Fryxell B. and Arnett D. (1991) Instability and clumping in SN 1987A. *Astron. Astrophys.* **251**, 505–514.

Nicolussi G. K., Davis A. M., Pellin M. J., Lewis R. S., Clayton R. N. and Amari S. (1997) *S*-Process zirconium in presolar silicon carbide grains. *Science* **277**, 1281–1283.

Nicolussi G. K., Pellin M. J., Lewis R. S., Davis A. M., Amari S. and Clayton R. N. (1998a) Molybdenum isotopic composition of individual presolar silicon carbide grains from the Murchison meteorite. *Geochim. Cosmochim. Acta* **62**, 1093–1104.

Nicolussi G. K., Pellin M. J., Lewis R. S., Davis A. M., Clayton R. N. and Amari S. (1998b) Zirconium and molybdenum in individual circumstellar graphite grains: New isotopic data on the nucleosynthesis of heavy elements. *Astrophys. J.* **504**, 492–499.

Nicolussi G. K., Pellin M. J., Lewis R. S., Davis A. M., Clayton R. N. and Amari S. (1998c) Strontium isotopic composition in individual circumstellar silicon carbide grains: A record of *s*-process nucleosynthesis. *Phys. Rev. Lett.* **81**, 3583–3586.

Niederer F. R. and Papanastassiou D. A. (1984) Ca isotopes in refractory inclusions. *Geochim. Cosmochim. Acta* **48**, 1279–1293.

Nittler L. R. (1996) Quantitative isotopic ratio ion imaging and its application to studies of preserved stardust in meteorites. Ph. D. thesis, Washington Univ., St. Louis.

Nittler L. R. and Hoppe P. (2005) Are presolar silicon carbide grains from novae actually from supernovae? *Astrophys. J.* **631**, L89–L92.

Nittler L. R., Amari S., Zinner E., Woosley S. E. and Lewis R. S. (1996) Extinct ^{44}Ti in presolar graphite and SiC: Proof of a supernova origin. *Astrophys. J.* **462**, L31–L34.

Nittler L. R., Alexander C. M. O'D., Gallino R., Hoppe P., Nguyen A. N., Stadermann F. J. and Zinner E. (2008) Aluminum-, calcium- and titanium-rich oxide stardust in ordinary chondrite meteorites. *Astrophys. J.* **682**, 1450–1478.

Nollett K. M., Busso M. and Wasserburg G. J. (2003) Cool bottom processes on the thermally pulsing asymptotic giant branch and the isotopic composition of circumstellar dust grains. *Astrophys. J.* **582**, 1036–1058.

Nomoto K., Thielemann F.-K. and Yokoi K. (1984) Accreting white dwarf models of Type I supernova. III – Carbon deflagration supernovae. *Astrophys. J.* **286**, 644–658.

Rauscher T., Heger A., Hoffman R. D. and Woosley S. E. (2002) Nucleosynthesis in massive stars with improved nuclear and stellar physics. *Astrophys. J.* **576**, 323–348.

Savina M. R., Pellin M. J., Tripa C. E., Veryovkin I. V., Calaway W. F. and Davis A. M. (2003) Analyzing individual presolar grains with CHARISMA. *Geochim. Cosmochim. Acta* **67**, 3215–3225.

Sharp C. M. and Wasserburg G. J. (1995) Molecular equilibria and condensation temperatures in carbon-rich gases. *Geochim. Cosmochim. Acta* **59**, 1633–1652.

Shields W. R. (1966) NBS Technical Note 277. U.S. Government Publishing Office, Washington, D.C.

Sloan G. C., Matsuura M., Zijlstra A. A., Lagadec E., Groenewegen M. A. T., Wood P. R., Szyszka C., Bernard-Salas J. and van Loon J. T. (2009) Dust formation in a galaxy with primitive abundances. *Science* **323**, 353–355.

Stadermann F. J., Croat T. K., Bernatowicz T. J., Amari S., Messenger S., Walker R. M. and Zinner E. (2005) Supernova graphite in the NanoSIMS: Carbon, oxygen and titanium isotopic compositions of a spherule and its TiC sub-components. *Geochim. Cosmochim. Acta* **69**, 177–188.

Starrfield S., Sparks W. M. and Truran J. W. (1985) Recurrent novae as a consequence of the accretion of solar material onto a 1.38 M_t white dwarf. *Astrophys. J.* **291**, 136–146.

Thielemann F.-K., Nomoto K. and Yokoi K. (1986) Explosive nucleosynthesis in carbon deflagration models of Type I supernovae. *Astron. Astrophys.* **158**, 17–33.

Thielemann F.-K., Nomoto K. and Hashimoto M.-A. (1996) Core-collapse supernovae and their ejecta. *Astrophys. J.* **460**, 408–436.

Timmes F. X., Woosley S. E. and Weaver T. A. (1995) Galactic chemical evolution: Hydrogen through zinc. *Astrophys. J. Suppl.* **98**, 617–658.

Timmes F. X., Woosley S. E., Hartmann D. H. and Hoffman R. D. (1996) The production of ^{44}Ti and ^{60}Co in supernovae. *Astrophys. J.* **464**, 332–341.

Travaglio C., Gallino R., Zinner E., Amari S. and Woosley S. (1998) Presolar dust grains from Type II supernovae: Mixing in the ejecta and silicon isotopic ratios. In *Nuclei in the Cosmos V* (eds. N. Prantzos and S. Harissopulos). Editions Frontières, Paris, pp. 567–569.

Travaglio C., Gallino R., Amari S., Zinner E., Woosley S. and Lewis R. S. (1999) Low-density graphite grains and mixing in type II supernovae. *Astrophys. J.* **510**, 325–354.

Wasserburg G. J., Boothroyd A. I. and Sackmann I.-J. (1995a) Deep circulation in red giant stars: A solution to the carbon and oxygen isotope puzzles? *Astrophys. J.* **447**, L37–L40.

Wasserburg G. J., Gallino R., Busso M., Goswami J. N. and Raiteri C. M. (1995b) Injection of freshly synthesized ^{41}Ca in the early solar nebula by an AGB star. *Astrophys. J.* **440**, L101–L104.

Wiescher M., Görres J., Thielemann F.-K. and Ritter H. (1986) Explosive hydrogen burning in novae. *Astron. Astrophys.* **160**, 56–72.

Woosley S. E. (1986) Nucleosynthesis and stellar evolution. In *Nucleosynthesis and Chemical Evolution* (eds. B. Hauck, A. Maeder and G. Meynet). Observatoire de Genève, pp. 1–195.

Woosley S. E., Taam R. E. and Weaver T. A. (1986) Models for Type I supernova – Detonations in white dwarfs. *Astrophys. J.* **301**, 601–623.

Woosley S. E. and Weaver T. A. (1995) The evolution and explosion of massive stars, II. Explosive hydrodynamics and nucleosynthesis. *Astrophys. J. Suppl.* **101**, 181–235.

Xu X. C., Amari S., Gyngard F., Zinner E. and Lin Y. (2012) Isotopic measurements of rare submicrometer-sized SiC grains from the Murchison meteorite. *Meteorit. Planet. Sci.* **47**, #5104 (abstr.).

Yoshida T. (2007) Supernova mixtures reproducing isotopic ratios of presolar grains. *Astrophys. J.* **666**, 1048–1068.

Yoshida T. and Hashimoto M. (2004) Numerical analyses of isotopic ratios of presolar grains from supernovae. *Astrophys. J.* **606**, 592–604.

Zinner E. and Jadhav M. (2012) Internal "isochrones" within presolar dust grains. *Lunar Planet. Sci. XLIII*. #1122 (abstr.).

Zinner E., Amari S., Wopenka B. and Lewis R. S. (1995) Interstellar graphite in meteorites: Isotopic compositions and structural properties of single graphite grains from Murchison. *Meteoritics* **30**, 209–226.

Zinner E., Nittler L. R., Gallino R., Karakas A. I., Lugaro M., Straniero O. and Lattanzio J. C. (2006a) Silicon and carbon isotopic ratios in AGB stars: SiC grain data, models, and the Galactic evolution of the Si isotopes. *Astrophys. J.* **650**, 350–373.

Zinner E., Amari S. and Jadhav M. (2006b) On the stellar sources of presolar graphite. In *Proceedings of the International Symposium* "*Nuclei in the Cosmos – IX*", June 25–30, 2006, CERN, Geneva. Proceedings of Science, PoS (NIC-IX) 019.

Zinner E., Gyngard F. and Nittler L. R. (2010) Automated C and Si isotopic analysis of presolar SiC grains from the Indarch enstatite chondrite. *Lunar Planet Sci. XLI*. #1359 (abstr.).

Associate editor: Jitendra Nath Goswami